Technical Memorandum 33-367

Final Report: Surveyor Full-Scale Spacecraft Antenna Measurement Program
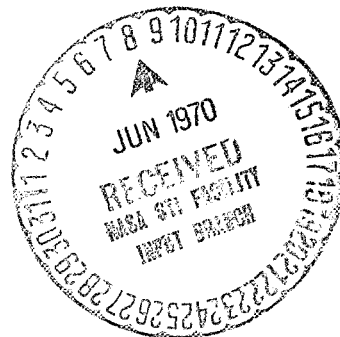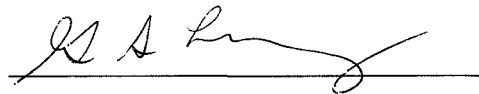
R. E. Herskind

N70-73957

NATIONAL AERONAUTICS AND SPACE ADMINISTRATION

Technical Memorandum 33-367

Final Report: Surveyor Full-Scale Spacecraft Antenna Measurement Program

R. E. Herskind

Approved by:

G. S. Levy, Manager
Communications Elements Research Section

JET PROPULSION LABORATORY
CALIFORNIA INSTITUTE OF TECHNOLOGY
PASADENA, CALIFORNIA

March 15, 1968

TECHNICAL MEMORANDUM 33-367

Copyright © 1968
Jet Propulsion Laboratory
California Institute of Technology

Contents

Contents (contd)

Tables

Figures

Contents (contd)

Figures (contd)

Abstract

With the aid of an accurate spacecraft model and the JPL calibrated antenna range, the *Surveyor* low-gain antenna pattern characteristics were remeasured with increased accuracy. Uncertainties were reduced on the order of 5.5 and 6.5 dB at the 0- and −10-dB levels, respectively.

The full-scale patterns of spherical coverage were recorded for *Surveyor* SC-1 configuration at 2295.0- and 2113.0-MHz frequencies. These patterns are on magnetic tape suitable for use in the telecommunication prediction program and are in microfilm analog form. Full-sphere patterns were also recorded at 2295.0 MHz for omni antenna A radiating in a stowed position with omni antenna B extended. Three analog *roll* patterns representing constant θ = 15, 35, and 60 deg were recorded for this stowed configuration at the 2113.0-MHz frequency.

Perturbation studies were conducted at 2295.0 MHz to demonstrate the solar panel-planar array and omni mechanical position tolerances on the spacecraft patterns. For the SC-2 model, one set of full-scale patterns of spherical coverage was obtained for the omni antenna A at 2295.0 MHz in the cruise mode. No antenna pattern data were recorded for the planar array antenna.

Final Report: *Surveyor* Full-Scale Spacecraft Antenna Measurement Program

I. Introduction

This report provides final information on the JPL program for the measurement of the *Surveyor* full-scale antenna patterns at the JPL 3300-ft antenna range. Details of subsystem measurements and calibrations are not included.

A full-scale *Surveyor* spacecraft RF-1 model (Fig. 1) was designed and built at JPL for the prime purpose of recording accurate full-scale spacecraft antenna patterns. The need for such a model and accurate measurements was determined, principally, by two factors:

(1) The *Surveyor* MA-2 spacecraft model originally used for full-scale pattern evaluation did not represent in detail, due to lack of definition at the time it was built, the final *Surveyor* SC-1 flight configuration.

(2) Original measurements made on the MA-2 model at Hughes Aircraft Co. contained measurement uncertainties which were considered excessive. These uncertainties were basically due to instrumentation errors and reflection errors caused by undesirable range geometry. All errors were accounted for principally by estimates and measured estimates.

For guidelines in the remeasurement program, a Task Description Control Document was written. This document proposed the recording of accurate patterns with the aid of the following:

(1) A more accurate full-scale antenna model spacecraft.

(2) The JPL 3300-ft antenna range. Use of the JPL antenna range aided in accomplishing the task objective by utilizing the following:

(a) Extensive component and system calibration procedures developed at JPL.

(b) Previously gained knowledge of the magnitude of departure from a plane wave of the illuminating field at the receiving site. The JPL range had fewer sources of error than the Hughes range due to more desirable range geometry conditions. Knowledge of the range errors was important since these errors constitute a major contribution to the overall uncertainties assigned to the pattern data.

(c) A digital antenna pattern (DAP) recording facility. This facility allowed patterns and associated tolerances to be recorded on magnetic tape to provide increased accuracy in performing *Surveyor* communications analysis.
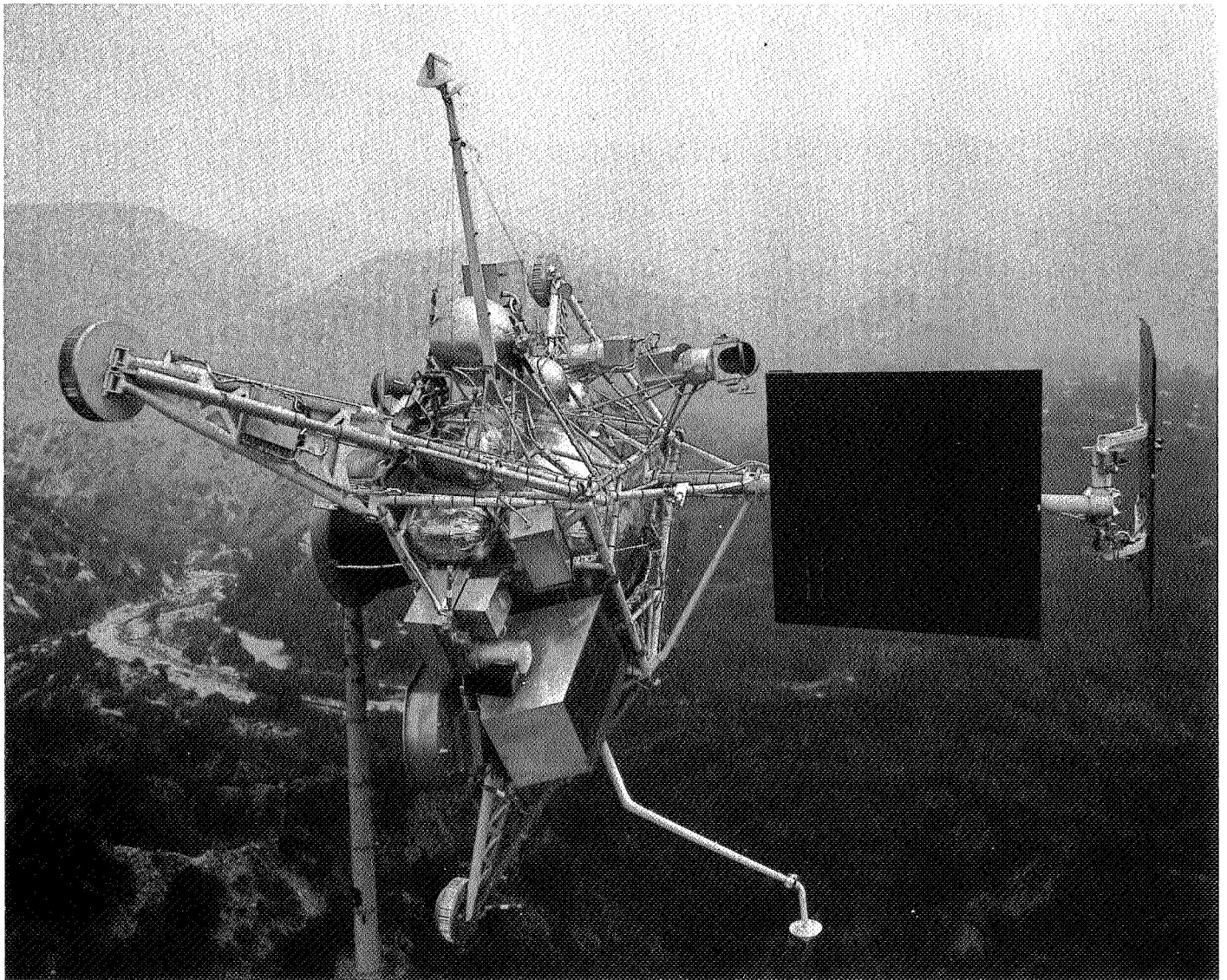
Fig. 1. *Surveyor spacecraft RF-1 model*

II. MA-2 Antenna Model Spacecraft

The MA-2 antenna model spacecraft, which was built by Hughes for the original pattern data, was brought to JPL where it was overhauled and modified for JPL support tower mounting. This antenna model was used during the program as a training tool for range and optics personnel in the establishment of:

(1) Measurement procedures for defining the locations of the omni antennas.

(2) Procedures for determining the spacecraft coordinate system.

(3) General calibration procedures for the recording of full-scale antenna patterns.

An unwritten secondary objective of obtaining full-sphere patterns for both antennas at two frequencies for the cruise mode was not realized on the MA-2 model, because of measurement instrumentation problems and scheduling commitments. One complete set of patterns was obtained for the omni antenna A cruise mode at 2295.0 MHz. In this sphere of pattern data, the patterns representing right-hand polarized constant clock angle cuts of $\phi = 56$ and 116 deg are not valid and should not be used. These patterns were found by the computer to be outside the specified angular tolerances. The computer requires data which are within tolerances before the data can be finally processed (see Section VI-D). Therefore, to satisfy scheduling commitments, no rerun of the bad patterns was made and the clock angles of 56 and 116 deg were dummied so that final processing might be carried out for this one set of patterns.

III. RF-1 Spacecraft

A. Design Objective

A study of the primary patterns of the omni antennas revealed that these antennas heavily illuminate the spacecraft structure. It was, therefore, judged that the secondary antenna patterns of the spacecraft could be perturbed by spacecraft appendages such as cables, substructure, and dielectric surfaces. It was determined that, for accurate antenna patterns, the spacecraft should be designed to represent as accurately as possible the nominal SC-1 configuration.

To assist in accomplishing this design objective, an RF-1 General Modeling Agreement was written and constituted the guidelines to which the model was built. In general, this document specified that the basic space-craft frame was to be constructed of 1020 steel with an *empty* substructure of lightweight aluminum. All cable harnessing and dielectric surfaces were dummied to approximate the flight specification. Flight type hardware was utilized where possible and when available. Major spacecraft components of flight type quality, actually used on the RF-1 model, consisted of the following items:

Item	Category of hardware
Solar panel	T-21 test model
Planar array	T-21 test model
Omni antennas, booms and associated RF cabling	T-21 test model
RADVS antennas	Engineering evaluation units
Canopus sensor shield	Engineering evaluation units
Crushable blocks	Class 3 test hardware
Retro nozzle	Scrap hardware

B. RF-1 Spacecraft Model Deflections—Analytical

To minimize measurement errors from the effects of spacecraft and spacecraft appendage deflections in a 1-g field, a theoretical analysis of elastic deflections was performed on the proposed RF-1 model. The analysis assumed the use of 1020 steel for the basic frame and lightweight aluminum for *empty* substructures.

The spacecraft appendages showing maximum elastic deflection were the omni antennas and the tip of the antenna solar panel positioner (ASPP) mast. Maximum omni antenna A deflection occurred for the case where the gravitational vector was along the x-axis ($-$z-axis in a horizontal plane) and was 0.142, 0.037, and 0.016 in. from nominal in the x-, y- and z-coordinates, respectively. The corresponding deflection for omni antenna B was 0.110, -0.042, and 0.014 in. from nominal in the x-, y-, and z-coordinates, respectively. The greatest deflection occurred at the solar panel hinge at the tip of the ASPP mast and was 0.254, -0.001, and 0.002 in. from nominal in the x-, y-, and z-coordinates, respectively.

The deflection analysis did not include the effects of gears and nonrigid coupling mechanisms. During the
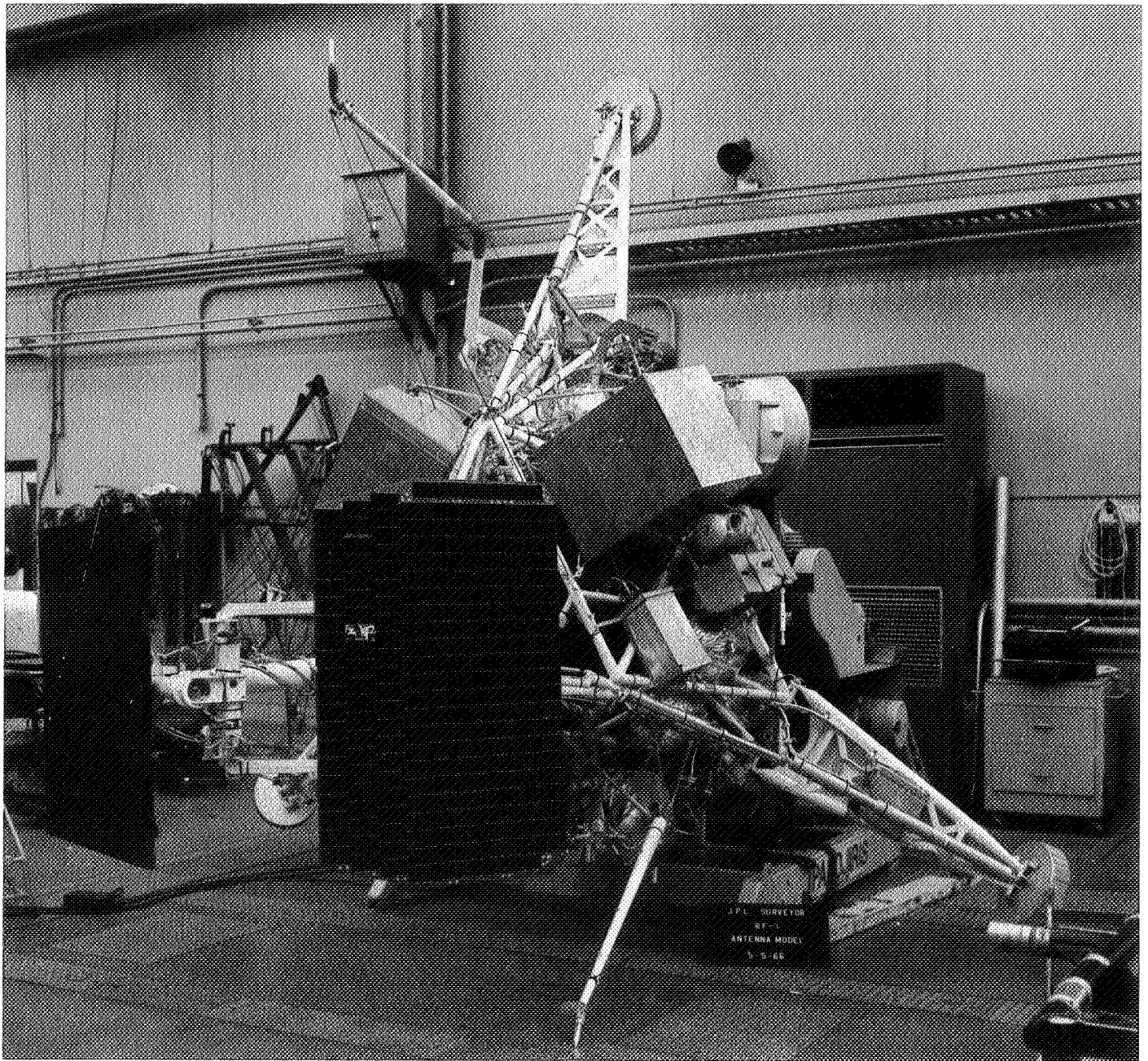
Fig. 2. RF-1 model rolled on z-axis (in horizontal plane)

pattern measurement program, deflections due to the omni antenna hinge mechanisms were minimized by using guy cords of 0.022-in. diameter with a fiberglass core.

C. Omni Antenna and ASPP Mast Deflection Measurements

1. Omni antennas. A measurement program was conducted in JPL Building 18 to determine the changes in the apex location of omni antennas in space as the spacecraft was rolled about the z-axis with the z-axis in a horizontal plane (Fig. 2). This z-axis orientation is the same as that used during the actual pattern tests. For these deflection measurements, dummied omni antennas of flight weight were used, since the omni antennas of the T-21 model were being evaluated on the antenna range. The results of this measurement program are tabulated in Figs. 3 and 4. The worst deflection for RF-1 omni antenna A occurred for the conical axis of omni antenna A in a horizontal plane ($\phi = 90$ deg with respect to the local vertical) and was -0.423 in. from nominal. The worst deflection of RF-1 omni antenna B occurred with omni antenna B inclined 30 deg from the local vertical and was 0.573 in. from nominal.

Fig. 3. Omni antenna A variation in coordinate locations vs change in spacecraft orientation
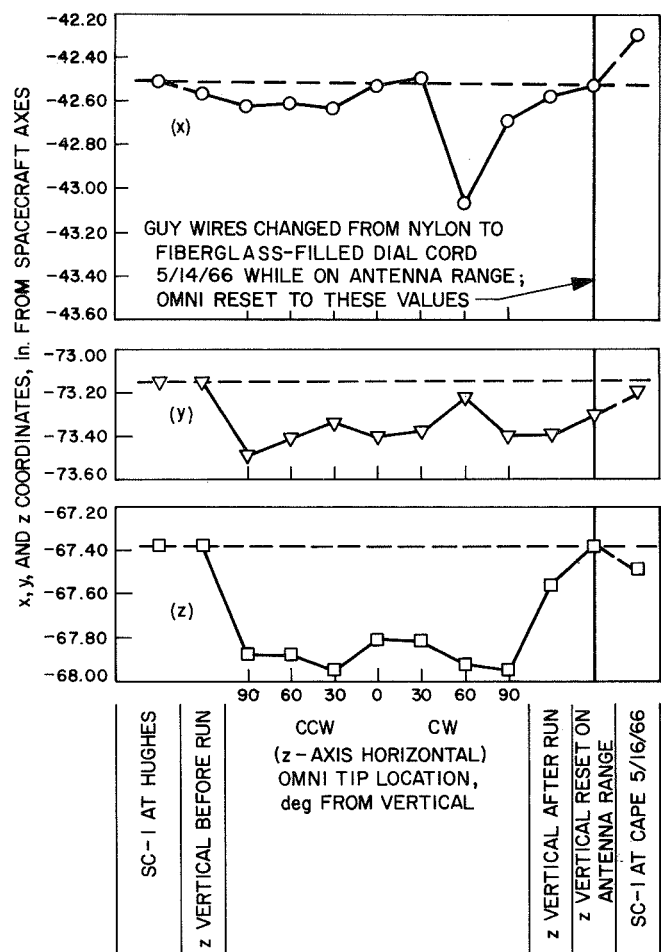
Fig. 4. Omni antenna B variation in coordinate locations vs change in spacecraft orientation

These measurements were performed with nylon guy cords and Teflon turnbuckles. Because of the general stretch characteristics of this nylon cord, a Dial cord with fiberglass core was considered more desirable for use as guy cords and was installed on the RF-1 spacecraft on the Mesa antenna range prior to recording final full-scale pattern data. It was assumed that the deviations during recording were less than those measured in Building 18. This assumption is derived from the less stretch experienced in the fiberglass core cord than in the nylon cord.

2. ASPP mast. For correcting ASPP mast elastic deflections, a steel turnbuckle arrangement was designed and installed in the tripod section of the ASPP mast. This mast was preset during final alignments before delivery to Building 18 for rotation deflection measurements.

Deflection measurements taken with the −z-axis in the horizontal plane (Fig. 2) revealed a maximum deflection of the ASPP mast tip of 0.385 in. about the −z-axis. This deflection was considered acceptable and no further adjustments were made.

The maximum tolerance for all optical measurements was determined by cognizant mechanical personnel to be ±0.032 in. Consideration was given to the temperature variations, the average thermal coefficients of expansion of fiberglass and steel, and the inherent capabilities of the optical instruments used. The effects of omni antenna position variations and the resultant perturbations on the spacecraft antenna pattern are covered in Section VII.

IV. Spacecraft Support Tower Design

The spacecraft support tower design was influenced by the *Surveyor* spacecraft configuration and by a constraint imposed upon the volume of space through which the antenna under test could traverse. The constraint was imposed by:

(1) The objective of obtaining patterns with minimum measurement uncertainties.

(2) The extreme low-gain characteristics of the omni antennas.

(3) The full-sphere pattern coverage requirement for the *Surveyor* spacecraft.

To minimize pattern measurement uncertainties, it was determined that, ideally, the omni antenna under test should not be positioned below the horizontal plane containing the spacecraft z-axis (Fig. 5), nor should the antenna enter the region behind the support tower as viewed from the transmitter. Entering these regions with the antenna would increase errors from range multipath in the case of below the horizontal plane and from support tower diffraction in the case of the region behind the support tower.

Hence, patterns should be recorded only in the upper front quadrant of an imaginary sphere surrounding the spacecraft as viewed from the illuminating antenna (Fig. 5). This restriction can be relaxed in some cases, depending upon the maximum allowable error. With this constraint as a guideline, two spacecraft support tower designs were considered:

(1) Option of support from both retro-motor or ASPP end.

(2) Single support from retro-motor end.

Study of design (1) showed that the antenna position constraint could be satisfied by recording one-half of the sphere with the spacecraft mounted from the retro-motor end, then swapping ends or mounting the spacecraft from the ASPP end for the other hemisphere.

It was determined by cognizant mechanical personnel, however, that support of the spacecraft by the ASPP end would produce elastic deflections of the ASPP mast greater than 1 in. and would require additional cantilever support devices to correct for such deflections.
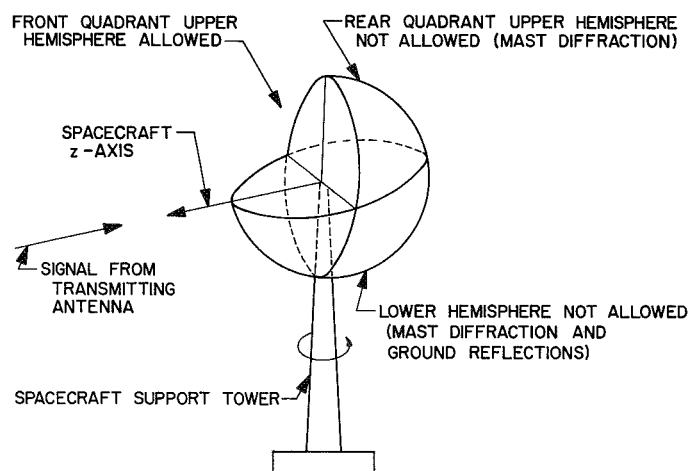
Fig. 5. Restricted regions of antenna position

Such elastic deflections were judged excessive from an antenna measurement point of view; also, any additional cantilever support devices would produce unrealistic ASPP mast configurations, which were judged unacceptable from an antenna pattern accuracy point of view. Mounting the spacecraft from its side via cantilevers was also considered for satisfying the antenna position constraints; however, because of spacecraft appendage locations, cantilever support devices could not be positioned for complete spherical coverage.

The next approach was that of alternative design (2), a single retro mounting. This approach required that the omni antenna position constraints be relaxed, since full-sphere coverage required the antenna under test to traverse the total volume represented by the upper hemisphere of Fig. 5. The principal drawback of this type of pattern is that a period of time exists when the support tower obscures the antenna under test.

A field probing study was performed at the JPL antenna range to assess the amount of distortion in a *Surveyor* antenna pattern when measured in the region behind the support tower. Results of the study showed that errors on the order of ±3.0 dB at the −10-dB levels of the primary pattern were possible. Since range errors constitute the major source of the total measurement uncertainty, this ±3.0 dB was considered as acceptable and as a contributor toward a significant decrease in the original full-scale pattern measurements.

Based on these results, the single support from the retro-motor end was studied further. Detailed study of
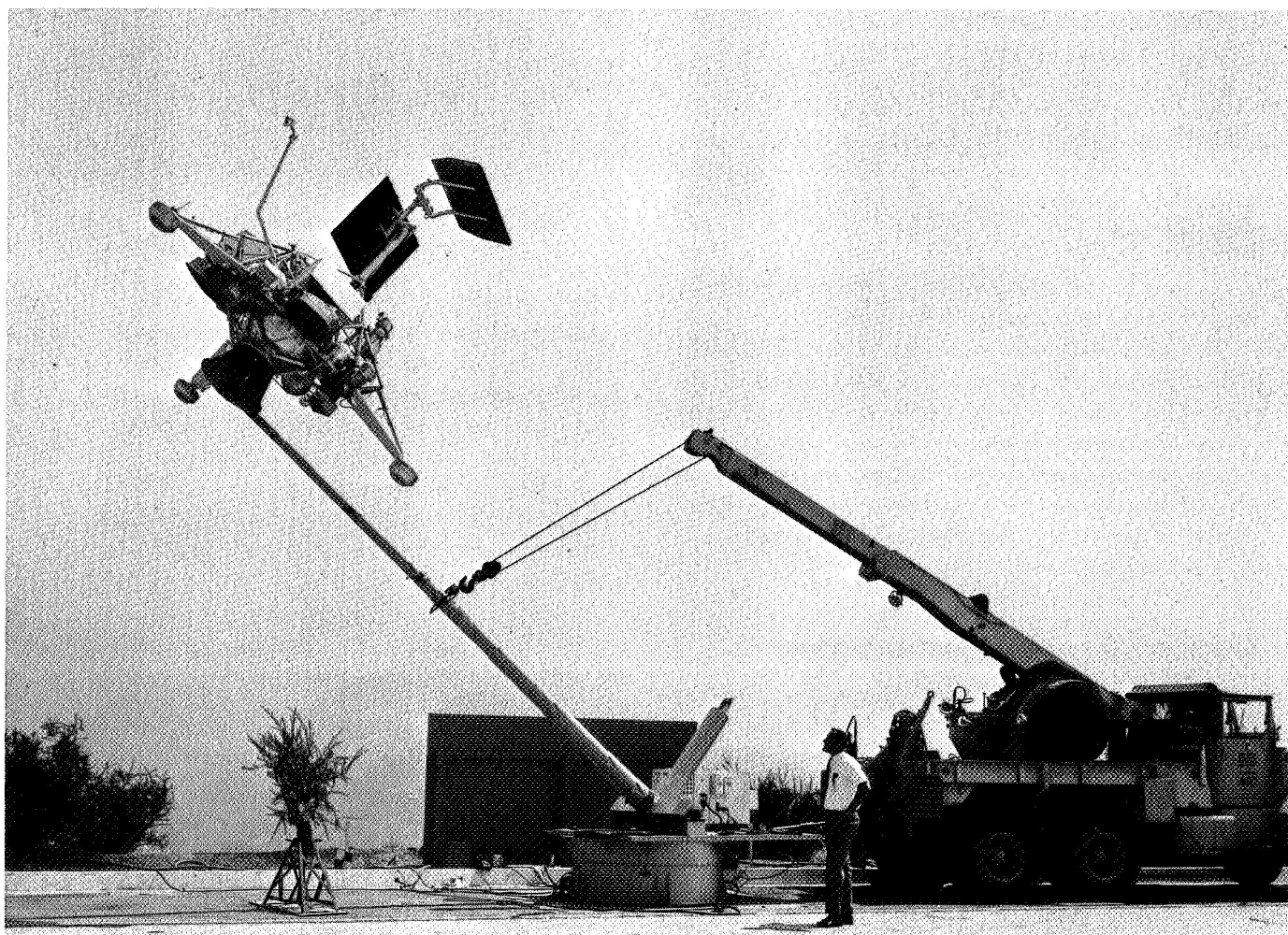
Fig. 6. Crane attachment to support tower with spacecraft

implementing the single retro mounting scheme revealed the following:

(1) Full-sphere pattern coverage could be accomplished by recording 0–180 deg in clock angle (roll) and 0–360 deg in cone angle (azimuth). Although the antenna under test now traverses the total upper hemisphere of Fig. 4 (a relaxation of the original specification), the requirement that the antenna remain above the horizontal plane is satisfied.

(2) Single retro mounting with reduced spacecraft handling and realignment would reduce the possibilities of damage to the spacecraft model and reduce the errors in the reestablishment of the coordinate system.

(3) The *Surveyor* retro-motor casing could be used to house the roll axis, dc drive motor, synchro transmitter, and associated cabling, thus, eliminating reflection errors from these items that are usually mounted on the support tower.

Based on these considerations, it was decided that, for a *Surveyor* type spacecraft, the single retro-end mounting was the most desirable. It was, therefore, adopted as the method of support for measuring the *Surveyor* full-scale patterns.

The support tower was designed to pivot vertically at the base for ease in mounting and servicing the spacecraft. The spacecraft was mounted with the support tower in the horizontal position and, then, raised to the measurement position by a crane pulling a cable attached to a point approximately midway up the mast (Fig. 6). This spacecraft support tower design, in conjunction with a mobile storage shed, afforded relatively quick and easy storing of the *Surveyor* model during emergency weather conditions.

V. Spacecraft Ground Support Equipment

Protection of the spacecraft was afforded by a mobile storage shed designed specifically for the *Surveyor* model. The shed was designed to withstand winds up to approximately 120 mph, to be water tight, and to be placed over the spacecraft while the spacecraft was still attached to the support tower in a horizontal position (Fig. 7). Tiedowns and heavy-duty jacks for emergency weather conditions were provided for stability. The mobile storage shed was needed on three or four occasions during rainy conditions.
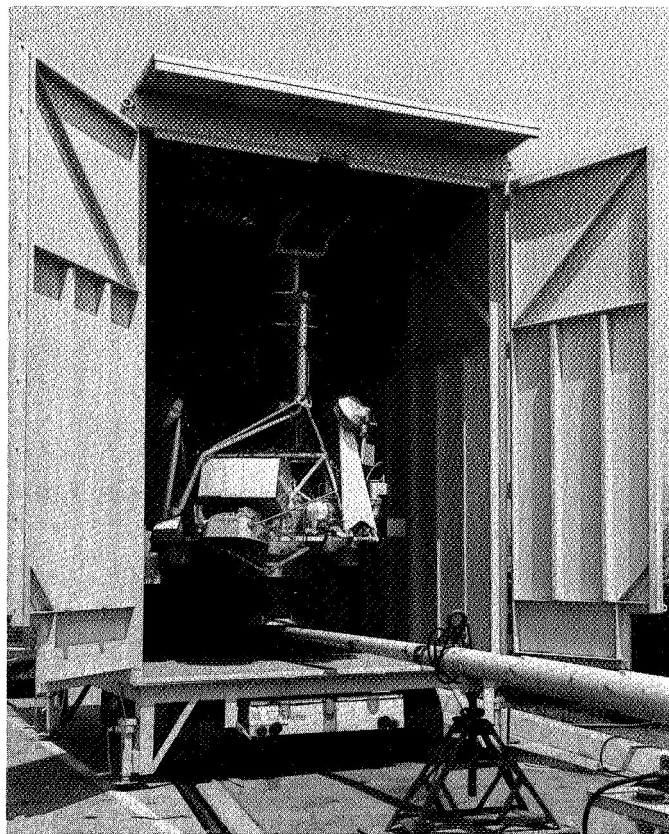
Fig. 7. Storage shed containing spacecraft on support tower

Additional ground support equipment in the form of a hydraulic jack was utilized. This jack was used during the crane raising operation to prevent *slamming* as the spacecraft center of gravity passed over the center of rotation, since the crane would lose *control* at that point. Conversely, on the lowering operation, the jack was used to *begin* the lowering operation until the spacecraft had passed over the center of rotation, at which time the crane assumed control.

VI. RF-1 Full-Scale Patterns

During pattern recordings, the RF-1 spacecraft model was located 3300 ft from the illuminating antenna and within 2.5 ft of the antenna elevation. The spacecraft was supported by the steel support tower previously described. A dc drive motor, synchro transmitter, rotary joint, cables, and associated hardware were hidden from electromagnetic view inside the *Surveyor* retro-motor shell (Fig. 8). This mode of spacecraft support allowed patterns to be taken 360 deg in the azimuth plane and

COMPARTMENT B

RETRO-MOTOR SHELL
AND NOZZLE

SYNCHRO BOX

RG-214

DRIVE
GEARS

DRIVE MOTOR (CLOCK ANGLE)

SPIROLINE
CABLE

RF ROTARY JOINT

RG-214

SPACECRAFT—z—AXIS

RG-214

STANDARD
GAIN HORN

RF CABLES

TO OMNI ANTENNA A

COMPARTMENT A

RG-214

TO OMNI ANTENNA B

RG-214

TO PLANAR ARRAY
(ALL THESE CABLES
FROM T-21 SPACECRAFT)

RG-214

SPACECRAFT
ATTACH
POINTS

CABLE MOUNTING BRACKET

RF CABLE N
ROUTED TO
STANDARD GAIN
HORN FOR GAIN
REFERENCE
MEASUREMENTS

ACCESS DOOR

SPIROLINE CABLE
TO RECEIVING SYSTEM

Fig. 8. Diagram of components in retro-motor shell and RF cabling routes

180 deg in the roll plane, yielding complete spherical coverage.

A. Spacecraft Coordinate System

The coordinate system used in the recording of the full-scale patterns is shown and described in Fig. 9. The method of recording antenna patterns conformed to the *orange peel* format with the clock angle ϕ held constant and the cone angle θ varied. Patterns were recorded on digital tape in 1- and 2-deg increments for cone and clock angles, respectively.
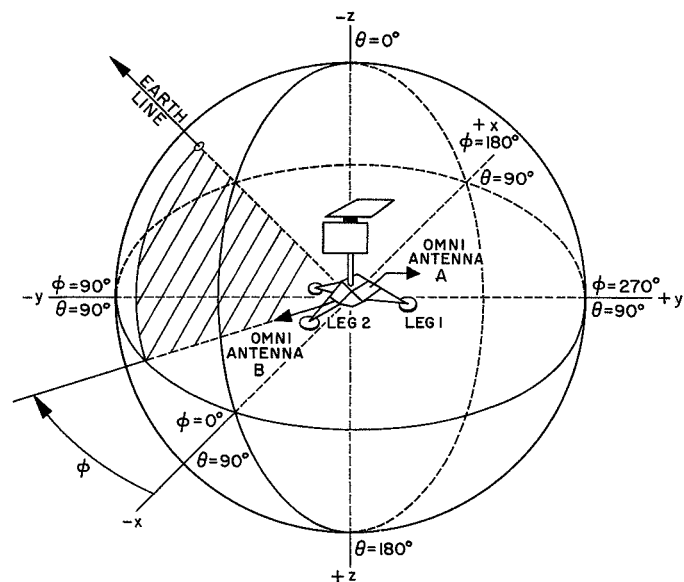
CANOPUS CLOCK ANGLE IS ANGLE BETWEEN EARTH-LINE PROJECTION ON SPACECRAFT COORDINATE x-y PLANE AND—x-AXIS, MEASURED IN CCW DIRECTION AS VIEWED FROM POINT ON—z-AXIS.

Fig. 9. Coordinate system for full-scale antenna measurements

The accuracy to which the coordinate system was established was derived by measurement of the tolerance contributors in Table 1.

To minimize errors due to range reflections and diffraction, the first spacecraft pattern cut was taken with the spacecraft rolled such that the axis of the omni antenna cone was parallel to the azimuth plane. The spacecraft was then rolled in 2-deg increments in a ccw direction (viewed from the illuminating antenna) such that the omni antenna under test was always above the horizon. This omni antenna position constraint precluded taking the first pattern at 0-deg clock angle in the space-

Table 1. Tolerance contributors and magnitudes

Tolerance contributor	Angle[a]	Tolerance magnitude, deg
Boresighted —z-axis to illuminating antenna	θ and ϕ	±0.04
Pattern tracking accuracy[b]	ϕ	±0.083
Azimuth turntable backlash	θ	negligible
Roll angle instability	ϕ	±0.2
Location of y-axis reference	ϕ	negligible
Measurement system error	θ and ϕ	±0.03

[a] θ total uncertainty = ±0.07 deg; ϕ total uncertainty = ±0.35 deg.

[b] Ability to maintain a constant clock angle while the cone angle is being cut.

craft coordinate system. Hence, for each antenna, the first cut represented a spacecraft coordinate clock angle differing from 0 deg by a constant.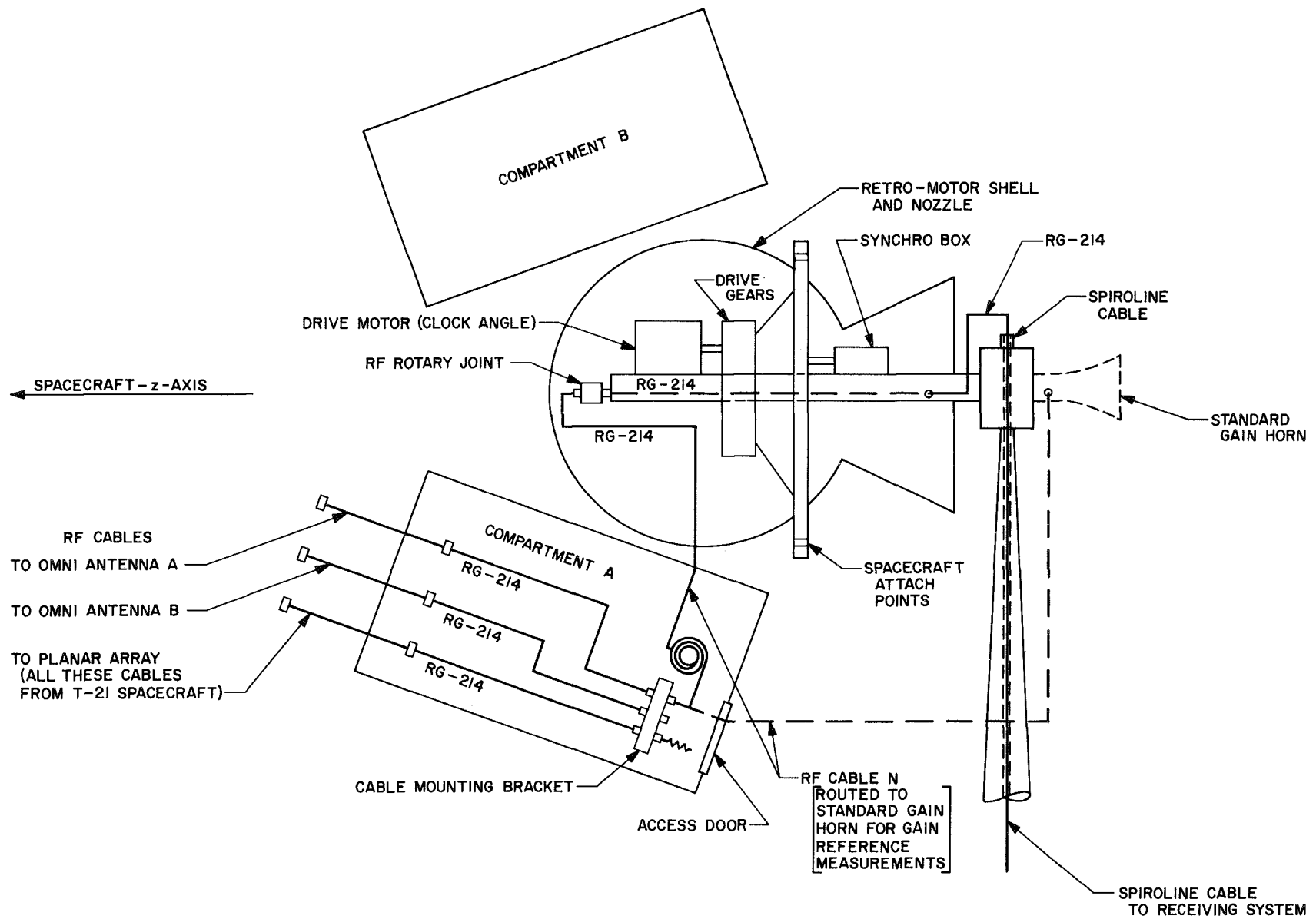 Since the DAP recorder records clock angles from 0–180 deg independent of the initial spacecraft roll orientation, a conversion was made to transform the DAP recorded angles into spacecraft coordinate angles. This conversion was accomplished in the computer program (discussed in a later section) for processing the raw antenna data.

B. Measurement Circuit

Recording of the full-scale *Surveyor* patterns was accomplished with the following circuit, shown in Fig. 10.

1. Illuminating system. The frequency source consisted of two crystal-controlled solid-state microwave oscillators tuned to 2295.000 and 2113.3125 MHz. RF power amplification was accomplished by a 10-W traveling-wave tube (TWT) amplifier operating at maximum power output. The grid of the TWT was square wave modulated at a 1-kHz audio rate. A rigid Heliax line provided signal transmission to a polarization box consisting of attenuators and phase shifters for obtaining right and left circular polarization. The output of the polarization generator was then fed directly into spatially orthogonal feeds of a 10-ft diameter parabolic antenna, having a gain at 2295.0 MHz of 34 dB.

2. Receiving system. The receiving end of the measurement circuit consisted of the spacecraft and receiving electronics.

SURVEYOR SPACECRAFT

10-ft diam ANTENNA

SPACE LOSS = -100.12 dB
AT R = 3450 ft, λ = 5.14 in.

ATTENUATOR

3-dB POWER SPLITTER

RCP
Δφ
Δ-dB
Δφ
LCP

RCP
Δφ
Δ-dB
Δφ
LCP

POLARIZATION BOX

TRANSMITTER MONITOR ANTENNA

SYNCHRO TRANSMITTER 1:1 36:1

BOLOMETER DETECTOR

SUPPORT TOWER

EQUIPMENT BOX

MODULATION MONITOR

POWER MONITOR

30 dB   30 dB   250-ft HELIAX
DIRECTIONAL COUPLERS

LOW PASS

POWER LEVEL CONTROL

TWT 2-4 kMHz

COAXIAL SWITCH

REMOTE UNIT

POWER LEVEL CONTROL UNIT

SQ. WAVE 1-kHz FORK

PADS

SOURCE
f = 2113.3125 MHz

CIRCULATOR

SOURCE
f = 2295.000 MHz

ILLUMINATOR SITE

VSWR METER

STRIP CHART
RECORDER $P(\phi, t) = kf(t)$

REMOTE COMMAND UNIT

DAP

CHART RECORDER

SYNCHRO ISOLATION AMPLIFIERS

POSITION CONTROL

CONTROL ROOM
BUILDING 212

SYNCHRO TRANSMITTER 1:1 36:1

LOWPASS FILTER

10-mW, 2-4 kMHz TWT

BANDPASS FILTER

dc BLOCK

BOLOMETER

BOLOMETER PREAMPLIFIER

SLIP RINGS

HIGH FIDELITY AMPLIFIER

600 Ω LOAD
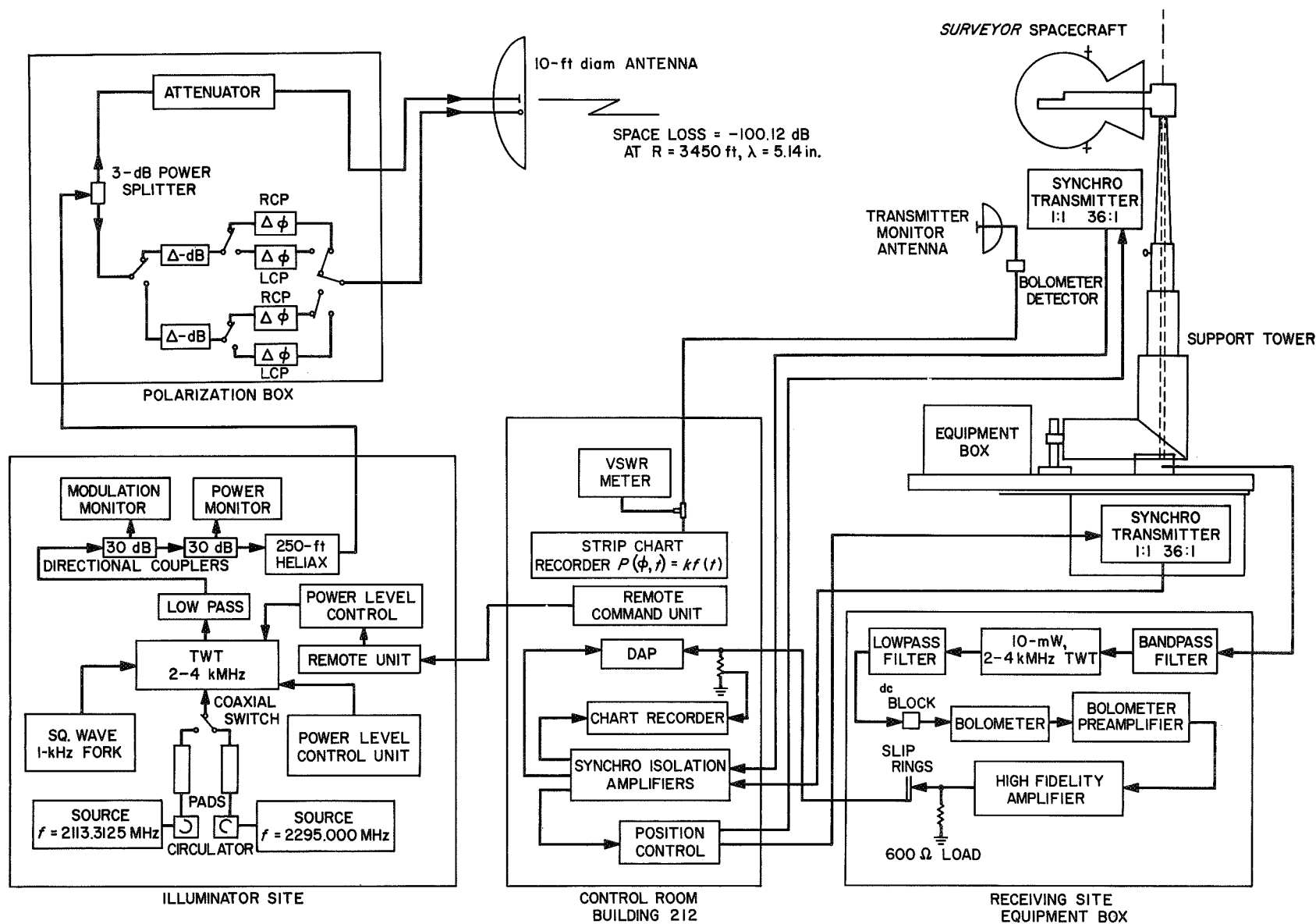
RECEIVING SITE
EQUIPMENT BOX

Fig. 10. Diagram of full-scale pattern measurement circuit

a. Spacecraft. Under flight conditions, the two omni antennas are terminated in a coaxial switch. Low isolation switches connected to several antennas can cause interference patterns to be generated. If the switches used on *Surveyor* had a low isolation, then they would have to be included as a part of the test configuration. An investigation of the switch isolations was made by Hughes personnel. Results of this investigation revealed typical switch isolation values in the order of 55 dB, with no switch isolation measuring below 50 dB. Therefore, the interferometer effects that could result were considered to be negligible over the major portion of the sphere with possible perturbations in the region of the nulls, the absolute levels of which are beyond the capability of being measured. Switches were not used for *Surveyor* RF-1 model. The receiving circuit between the omni antennas and the receiving electronics was as shown in Fig. 8. The omni antenna not under test was left in an open circuit condition as per flight configuration, and the planar array terminated in a 50-Ω load.

Cabling between the omni antennas and the mounting bracket in spacecraft compartment A was connected into the receiving system with cable N (Fig. 8) which exited compartment A, entered the retro-motor, and terminated in the rotary joint. The rotary joint was connected to a length of RG-214 cable and a 25-ft length of low loss Spiroline, completing the RF signal path to the receiving electronics box.

b. Receiving electronics. The RF Spiroline and the dc auxiliary cables were routed down the center of the mast before entering the receiving electronics located on the rotator. From the rigid Spiroline at the bottom of the support tower, the RF signal was fed through a bandpass filter and into a 10-mW traveling-wave tube amplifier. The signal was then detected by a bolometer, and the resulting audio signal was amplified with a 75-W audio amplifier. This signal was coupled to the azimuth rotator slip rings and transmitted by a hard line to the control room as input to the DAP and analog recorders. The recorded output consisted of spacecraft antenna pattern data in a digital magnetic tape format as well as in conventional analog form.

C. Summary of Pattern Recording Calibration Procedures

Calibration for each set of full-scale patterns was accomplished by the following procedures.

1. Illuminating antenna ellipticity. The illuminating antenna ellipticity was first measured with the aid of a rotating linear horn. Ellipticity measurements were made for both right-hand circular polarization (RCP) and left-hand circular polarization (LCP). Ellipticities were corrected as necessary, to values under 0.25 dB. Establishing low ellipticities at both polarizations was necessary to minimize the error in establishing relative power levels when transmitting either RCP or LCP.

2. Relative signal levels of illuminating antenna. A dual-polarization high-gain horn (21.8 dB at 2295.0 MHz) was mounted on the support tower to the rear of the spacecraft and boresighted to the transmitter (Fig. 11). A recording was made of the relative signal strength of the illumination while the illuminator and dual-polarized high-gain horn were both tuned to RCP and then to LCP. The relative levels in dB were later used as inputs to the computer program for calculation of worst case ellipticities.

3. Standard gain reference. With the dual-polarization high-gain horn boresighted to the transmitter, an absolute gain reference level was established at RCP. This step was accomplished by padding the dual-polarization high-gain horn to a level compatible with the expected spacecraft pattern gain and connecting cable N (Fig. 8) to the dual-polarization high-gain horn (Fig. 11). The corresponding DAP recorder voltage was then recorded as a *gain reference* voltage.

The established gain level was referenced to the input of the antenna cable mounting bracket at compartment A. This reference gain was adjusted in the final data to represent the gain as referenced to the omni antenna terminals by adding the accurately measured cable insertion and antenna mismatch losses.

D. Computer Processing Flow Chart

A flow diagram depicting the processing of raw antenna pattern data is shown in Fig. 12. Referring to the figure, a magnetic tape of RCP or LCP pattern data from the Mesa Antenna Range Facility (both RCP and LCP are required for the final data), is put through a computer test which is called a *blast routine*. The output of this program lists those particular pattern cuts (constant clock angles) that need to be rerun, if any, due to failure to pass predetermined standards of recording.

Among the checks run by the computer are the following:

(1) Check that the recorded angles (θ, ϕ) are within their specified tolerances.
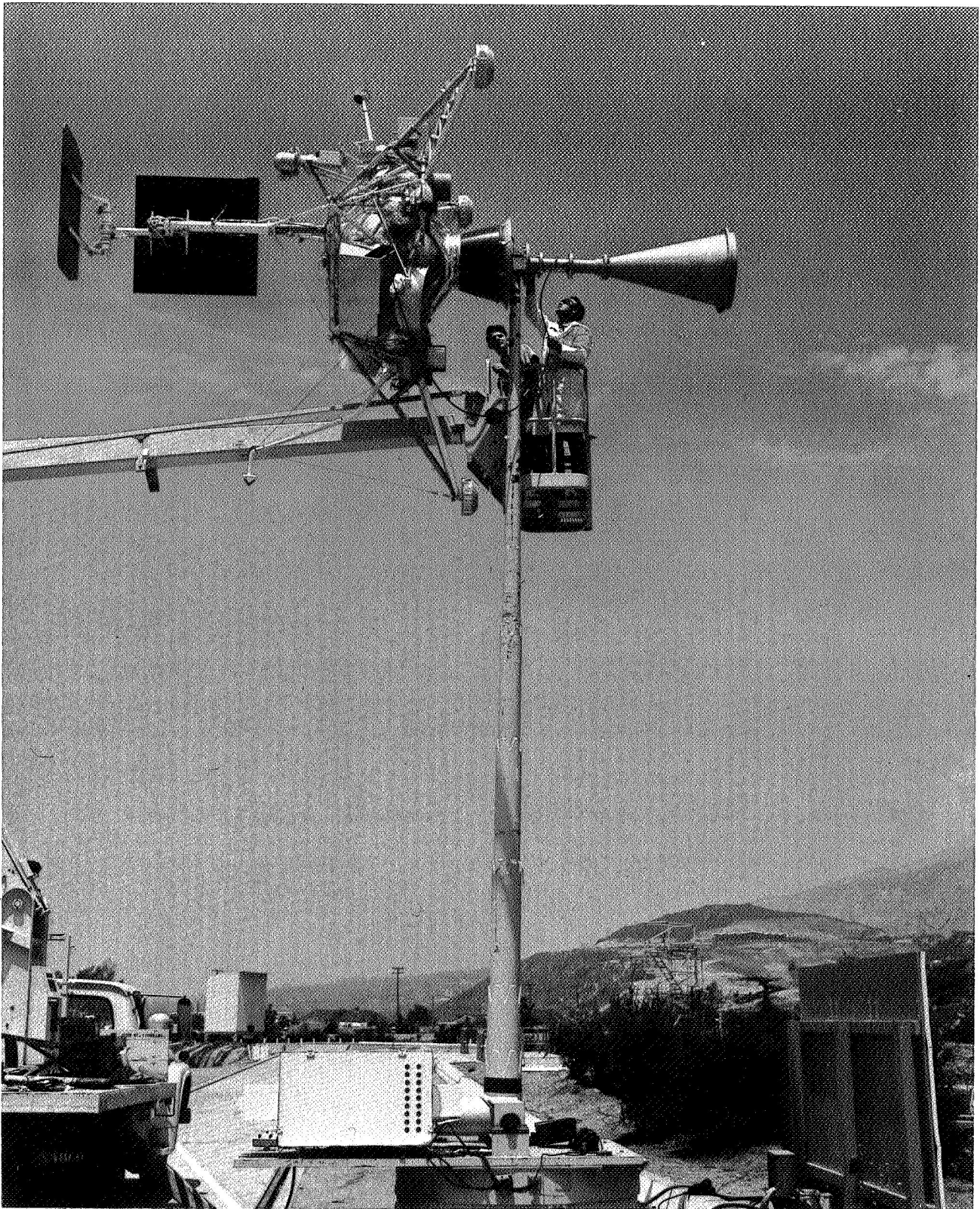
Fig. 11. Installation of dual-polarization high-gain horn onto support tower

PUNCH CARD INPUT INSTRUCTIONS

RECORDING MODE; START ANGLES; SAMPLE INCREMENTS; STOP ANGLES	INSERT RECORD NOS.; ORIGINAL TAPE NO.; INSERT TAPE NO.; DUPE TAPE NO.	ILLUMINATOR RCP AR;* ILLUMINATOR LCP AR; RCP-LCP POWER GAIN RATIO; GAIN SCALE FACTORS; TOLERANCE DATA; SPACECRAFT CONFIGURATION	NO PLOTS; PLOT ALL RECORDS; PARTIAL PLOT RECORD NOS.; PLOT LEGEND

MESA ANTENNA RANGE FACILITY

LCP AND/OR RCP LOW DENSITY DAP INPUT TAPE

FIRST TRY

INSERT

DUPE TAPE

ADDITIONAL TRIES

BLAST ROUTINE
(CHECKS PERFORMED)

CONSECUTIVE SKIPPED SAMPLES, CONSTANT ANGLE TOLERANCE, END OF RECORDS, ETC. (APPROXIMATELY 20 CHECKS)

PRINT OUTPUTS

LIST OF RECORDS THAT MUST BE RERUN

OR

STATEMENT THAT NO RECORDS NEED TO BE RERUN

TABULATION OF FIRST RECORD IN ENGLISH

RCP AND LCP (BOTH REQUIRED)

CLEAN ROUTINE

ANGLE TRANSFORMS; CONVERSION TO dB; COMPUTE TOLERANCE; COMPUTE ELLIPTICITY

HIGH DENSITY OUTPUT TAPE

USED AS EDCOM INPUT

RERUN RECORDS ON LOW DENSITY DAP INPUT TAPE

MESA ANTENNA RANGE FACILITY

USED TO CHECK AGAINST SIMULTANEOUSLY RECORDED ANALOG PATTERNS

ROLLED PLOTS

4020 PLOTTER

PLOT TAPE (SCRATCH)

USED AS PROJECT DOCUMENTATION

BOUND PLOTS

REPRO

MICROFILM PLOTS

*AR = AXIAL RATIO

Fig. 12. Diagram of raw antenna pattern data processing

(2) Check that the number of skipped data samples is less than a specified minimum.

(3) Check for any parity errors.

If the answers to these and other format checks are correct for both a right- and left-hand polarized tape, both tapes are then processed in the *clean* routine. This *clean* routine converts the relative gain levels to absolute gain in dB, computes tolerances and ellipticity, and raises the resultant data to a higher density format. This tape is then used as the input to the communications predictions programs. Also, the output of the *clean* routine is used to generate analog and microfilm plots.

The computer program for processing the low density tapes required two modifications to make it compatible with *Surveyor* requirements. The first modification was made to the recorded clock angles. As discussed previo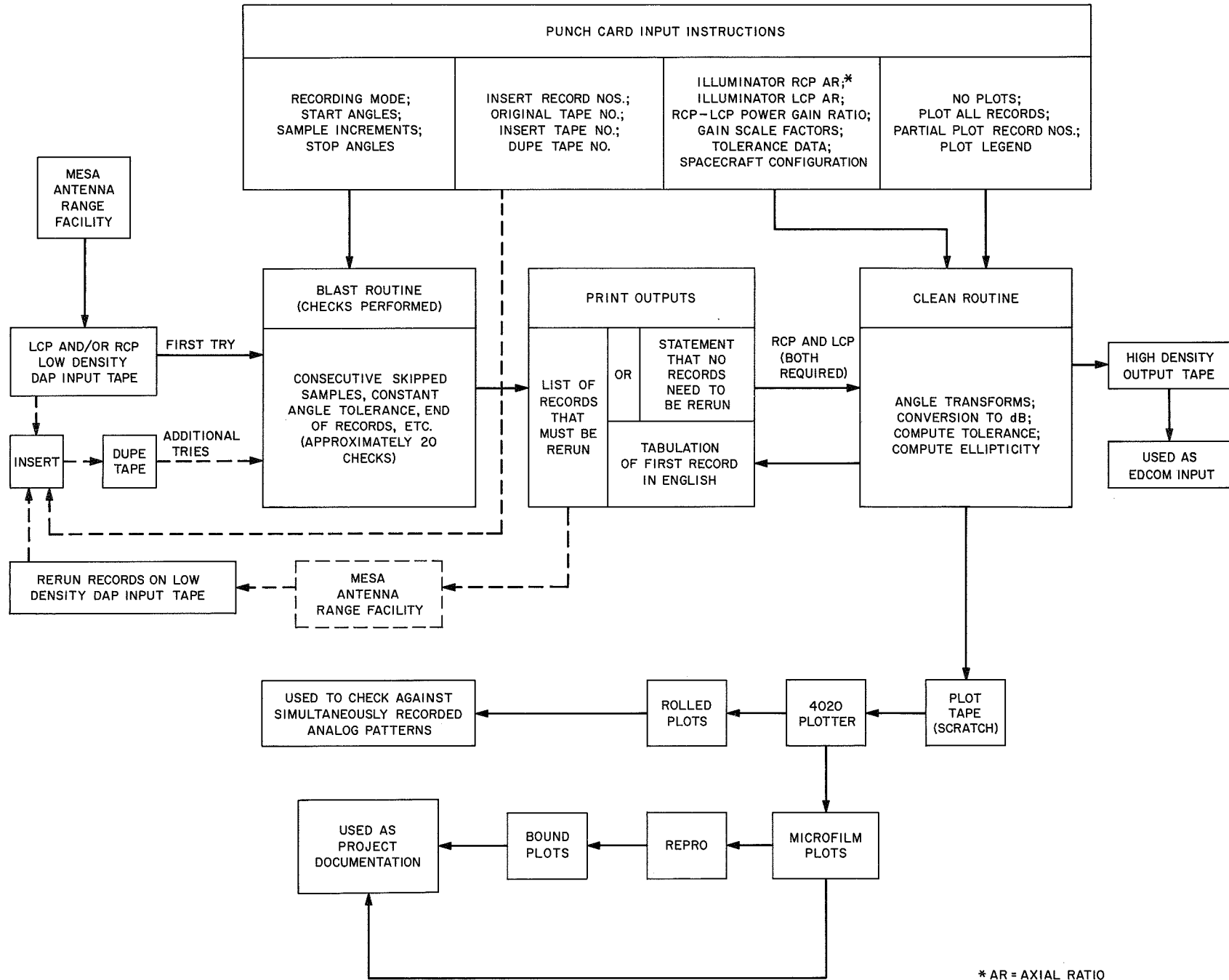usly, the omni antenna while under test was restricted to assume positions in the upper hemisphere of an imaginary sphere located about the spacecraft. The consequence of this restriction was that the recorded clock angles for each antenna differed from the spacecraft coordinate clock angles by a constant; the value of the constant depended upon the location of the omni antenna on the spacecraft. Therefore, the computer program was modified to convert the recorded clock angles to actual spacecraft coordinate clock angles. For omni antennas A and B, the clock angle constants were 269.50 and 59.27 deg, respectively.

The second modification to the computer program was made to the pattern tolerancing format. Previous to the modification, tolerances on antenna patterns were expressed as a constant plus a linear gain dependent variable, i.e.,

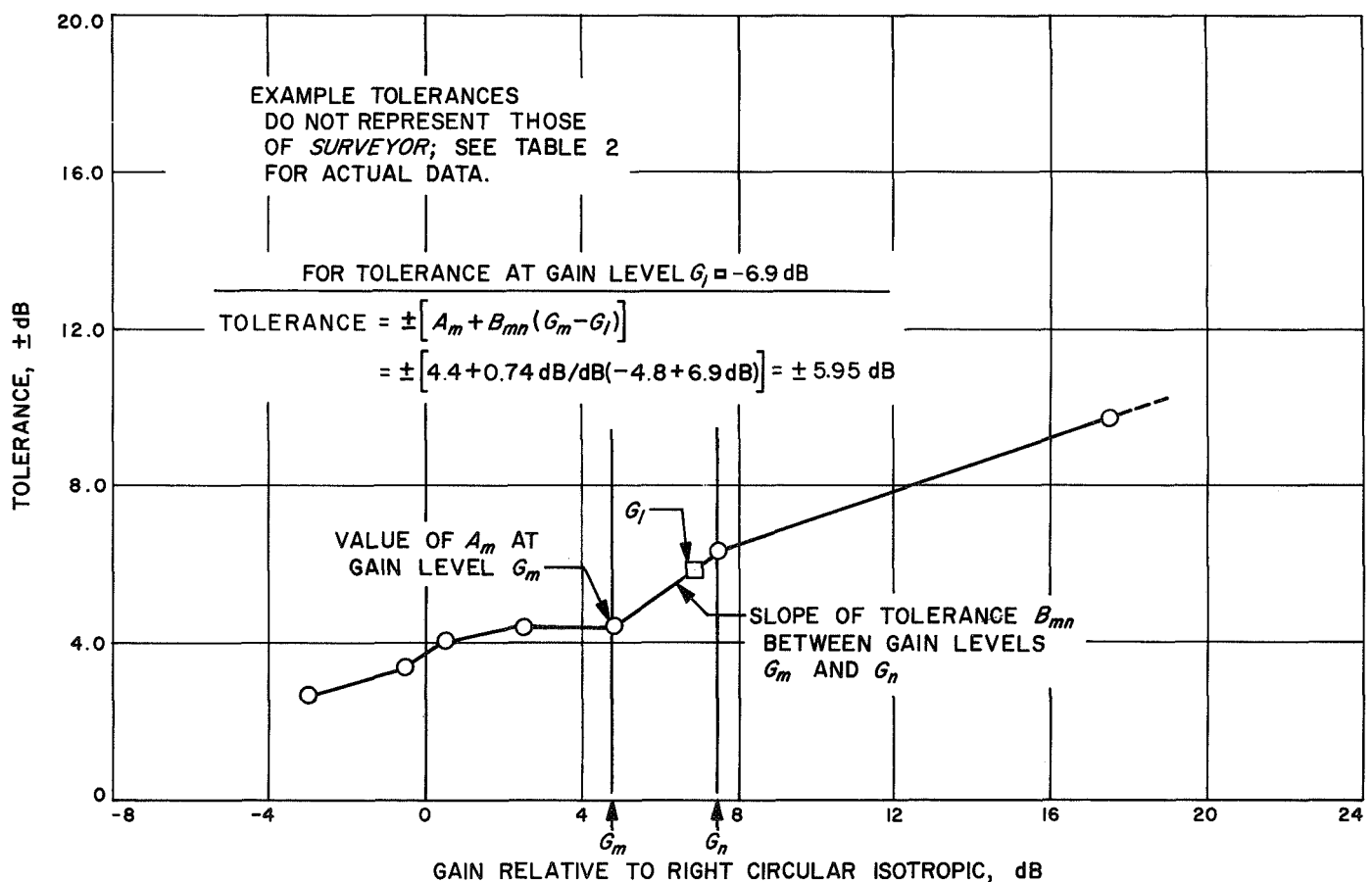$$\text{Tolerance} = \pm [A + B (G_o - G)]$$

Fig. 13. Example of sectionally continuous tolerancing

where

A = value of tolerance at peak of pattern

B = slope of tolerance function

G_o = gain at peak of pattern

G = gain level at which tolerance is being evaluated

For *Surveyor* patterns, this tolerance format was altered to include constants and slopes, both as a function of gain level. The need for a new format arose due to the sectionally continuous character of the range errors as a function of gain level. These range errors are fully discussed in the section on tolerances. The new format (Fig. 13) is described as:

$$\text{Tolerance} = \pm [A_m + B_{mn} (G_m - G_l)]$$

where

A_m = constant value assigned to tolerance at gain level G_m

B_{mn} = slope of tolerance function in gain region bounded by G_m and G_n (units of B_{mn} are dB/dB)

$(G_m - G_l)$ = difference between gain levels G_m and G_l in region bounded by G_m and G_n

$$G_m \leq G_l < G_n$$

This method was defined as *sectional tolerancing*.

E. Pattern Data Recorded

Original task objectives, which included full-scale patterns for the SC-2 spacecraft, were not entirely realized. A complete set of cruise mode data was recorded for the SC-1 configuration. However, no planar array pattern was obtained.

VII. Tolerances

Tolerances placed on the measured antenna pattern data result from the following sources of error:

(1) Range reflection and diffraction.

(2) Instrumentation calibration.

(3) Spacecraft appendage position tolerances.

(4) Spacecraft appendage manufacturing and assembly tolerances.

Each of these sources of error is discussed in the following paragraphs.

A. Range Reflection and Diffraction

Range reflection and diffraction errors constitute the largest contributor to the total measurement uncertainty. The range errors are due primarily to multipath transmission caused by reflection from the surrounding terrain, and by diffraction from the canyon ridge edge in front of the spacecraft. These errors cause a nonuniform illumination at the receiving site, producing uncertainties in the measured pattern data. Included in the category of range errors is the error contributed by the support tower.

To determine the magnitude of measurement uncertainties due to range reflection and diffraction, it was necessary to probe the field in the vicinity of the receiving aperture. The exact method of probing the field for the extremely low-gain *Surveyor* antenna was the subject of much discussion between Hughes and JPL. It was concluded that, ideally, uncertainties would be maximally defined by a detailed field probing with the actual spacecraft at various positions in the field relative to the natural diffraction ridge (canyon wall) and the spacecraft support tower. Such a method, however ideal, was considered outside the limits of budget, equipment, and scheduling constraints. The plan adopted was the following:

A *Surveyor* prototype omni antenna was mounted on a fiberglass pole (Fig. 14) such that its conical axis was located in a horizontal plane. Its pointing angle α and radial distance R_o from the support tower simulated the position of omni antenna A when actually mounted on the spacecraft model. This omni antenna orientation also simulated the pattern cut through the apex of the omni antenna, and was considered as a worst case pattern since it possessed regions of low gain. Also, all other pattern cuts would be taken with the omni antenna apex increasingly pointing away from the earth, providing increasing discrimination to unwanted multipath reception by positioning the antenna null towards the earth. All range probing was, therefore, done for this worst case antenna orientation.

Data for obtaining range quality information were obtained by, first, taking a pattern cut of the prototype omni antenna in the nominal position described. Then additional patterns were recorded for:

(1) Radial distances about the nominal in increments of plus or minus a quarter wavelength, covering a total radial distance of one wavelength.
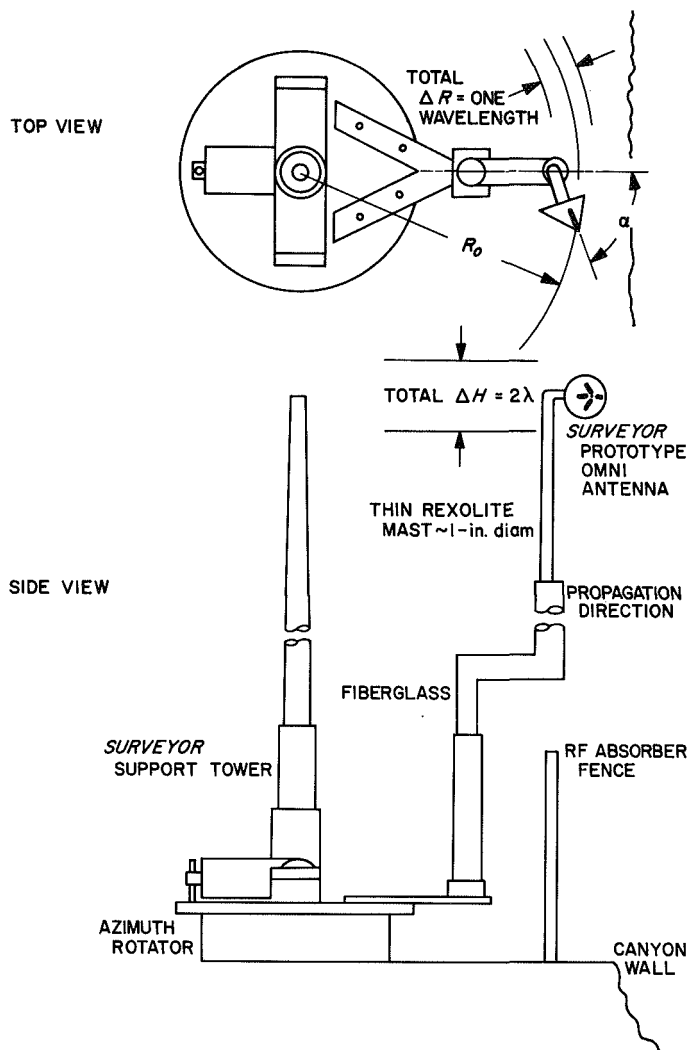
Fig. 14. Diagram of prototype omni antenna test setup for field probing

(2) Vertical distances in increments of plus or minus a quarter wavelength about the nominal for each radial distance.

The total vertical distance covered was approximately two wavelengths.

Also, data were collected for the nominal position of omni antenna B. Measurements representing radial and vertical distances about the nominal were made only to the extent of verifying that the field variations were similar for both antenna positions.

The resulting data included over 130 omni antenna prototype patterns, each representing various positions relative to the spacecraft support tower and the reflect-

ing terrain. Each of these patterns was traced onto a single chart, forming a composite pattern. An envelope enclosing all patterns on the chart was then drawn. Inspection of the composite pattern revealed that a reasonable random type error was present. The equivalent *free space* omni antenna pattern was then computed by drawing an average pattern of the composite pattern. The upper and lower bounds of the composite pattern envelope represent the positive and negative tolerance as a function of relative gain level due to the support tower and range reflections and diffractions. Figure 15 shows a comparison made between an average *free space* pattern of the omni antenna prototype taken on the Blaine range (a relatively *clean* range) and the average *free space* pattern derived from the field probing measurements. The patterns are compared in a best fit sense, since pattern shape (rather than absolute gain) is the basis of the comparison.

From the plot of Fig. 15, a symmetrical tolerance for range reflection and diffraction was derived. Figure 16 is a plot of this tolerance as a function of absolute gain level. This curve was derived by plotting one-half of the difference, in dB, between the upper and lower boundary curve (Fig. 15) at all values of absolute gain level vs gain level. Since the pattern of Fig. 15 is not perfectly symmetrical, a particular gain level may display different boundary separation values at two different angles of the pattern. Where these dual values occurred, the largest separation value in dB was used for computing the symmetrical tolerance.

For computer program purposes, Fig. 16 was arbitrarily adjusted to be a monotonically increasing function. The adjusted curve (solid line) is, therefore, slightly pessimistic.

The values of range tolerance at gain levels of +3 and +4 dB were linearly extrapolated, since the gain of the primary pattern was less than approximately +0.5 dB for the pattern cut taken. The arrows of Fig. 16 define regions of constant *slope*. (Tolerances at gain values in these regions are computed, as illustrated previously in Fig. 13, after all other tolerance contributions have been added as in Table 2.)

1. Supplementary data. The method of field probing described does not include the effects of a change in environment when the spacecraft is introduced between the antenna and support tower. To increase the confidence factor in the omni prototype antenna probing,
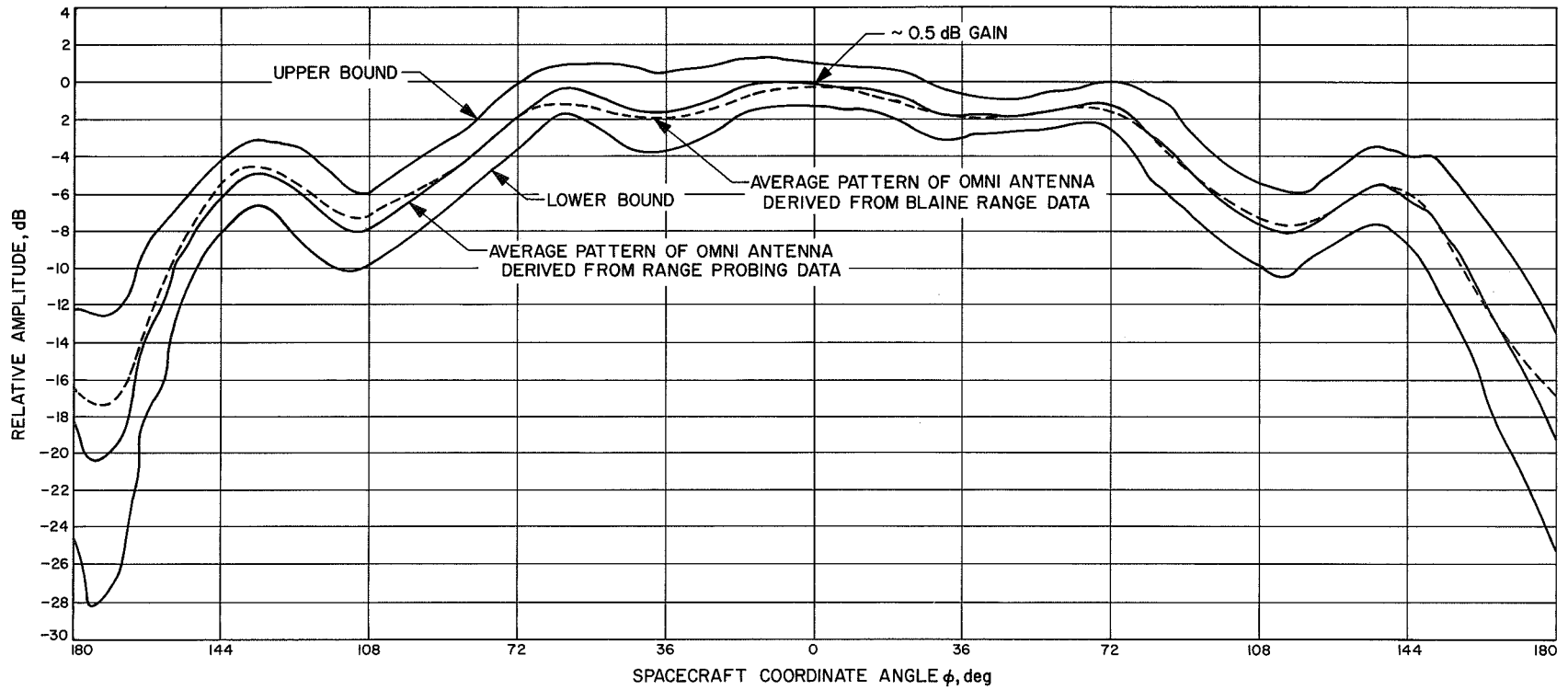
Fig. 15. Comparison of average pattern by field probing and Blaine range measurements

Table 2. Summary of measurement type tolerances for omni antennas A and B at 2113.3 and 2295.0 MHz

Tolerance factor	Frequency, MHz	Omni antenna	Derivation method	Constant value, dB	Sectionally continuous gain regions,[a] dB						
					3 to 0.5	0.5 to −0.5	−0.5 to −2.5	−2.5 to −4.8	−4.8 to −7.5	−7.5 to −17.5	Less than −17.5
Recording system linearity	2113.3	A	Meas	—	0 + 0.01	0.03 + 0.01	0.04 + 0.01	0.06 + 0.01	0.08 + 0.01	0.11 + 0.01	0.21 + 0.01
		B			0 + 0.01[b]	0.04 + 0.01	0.05 + 0.01	0.07 + 0.01	0.09 + 0.01	0.12 + 0.01	0.22 + 0.01
	2295.0	A-B	Meas	—	0 + 0.01	0.03 + 0.01	0.04 + 0.01	0.06 + 0.01	0.08 + 0.01	0.11 + 0.01	0.21 + 0.01
RF-1 spacecraft stability	Both	A	Meas	—	0.36	0.36	0.36	0.36	0.36	0.36	0.87
		B			0.17[c]	0.17	0.17	0.17	0.17	0.17	0.45
RF-1 pattern repeatability	Both	A	Meas	—	0.76	0.76	0.76	0.76	0.76	1.36	3.43
		B			0.69[c]	0.69	0.69	0.69	0.69	1.47	4.05
Range reflection and diffraction	2113.3	A	Meas	—	1.12 + 0.30	1.87 + 0.60	2.47 + 0.20	2.87 + 0.0	2.87 + 0.48	4.17 + 0.27	6.87 + 0.42
		B			0.83 + 0.30	1.87 + 0.60	2.47 + 0.20	2.87 + 0.0	2.87 + 0.48	4.17 + 0.27	6.87 + 0.42
	2295.0	A	Meas	—	0.65 + 0.30	1.40 + 0.60	2.00 + 0.20	2.40 + 0.0	2.40 + 0.48	3.70 + 0.27	6.40 + 0.42
		B			1.12 + 0.30[b]	1.87 + 0.60	2.47 + 0.20	2.87 + 0.0	2.87 + 0.48	4.17 + 0.27	6.87 + 0.42
Recording system stability	Both	A-B	Meas	±0.25							
Transmitter ellipticity stability	Both	A-B	Meas/est	Negligible							
Gain standard absolute calibration	2113.3	A-B	Meas	±0.20							
	2295.0			±0.15							
Gain comparison calibration	Both	A-B	Meas	±0.10							
Omni cable insertion loss	2113.3	A-B	Meas	±0.03							
	2295.0		Calc								
Polarization loss, absolute gain calibration	Both	A-B	Calc	Negligible							
Rotary joint wow	Both	A-B	Meas	±0.03							
Slip ring wow	Both	A-B	Meas	Negligible							
Wind modulation <5 mph	Both	A-B	Meas/est	±0.10							
Thermal distortion	2113.3	A-B	Est	Negligible							
	2295.0	A	Est	±0.2							
		B		Negligible							
Illuminator spacecraft interaction	Both	A-B	Calc	Negligible							
Totals[d]	2113.3	A	—	—	2.95 + 0.31	3.73 + 0.61	4.34 + 0.21	4.76 + 0.01	4.78 + 0.49	6.71 + 0.28	12.09 + 0.43
		B	—	—	2.40 + 0.31[b]	3.48 + 0.61	4.09 + 0.21	4.51 + 0.01	4.53 + 0.49	6.64 + 0.28	12.30 + 0.43
	2295.0	A	—	—	2.63 + 0.31	3.41 + 0.61	4.02 + 0.21	4.44 + 0.01	4.46 + 0.49	6.39 + 0.28	11.77 + 0.43
		B	—	—	2.64 + 0.31	3.42 + 0.61	4.03 + 0.21	4.45 + 0.01	4.47 + 0.49	6.58 + 0.28	12.24 + 0.43

[a] $X + Y = X$ dB + Y dB/dB.

[b] Omni antenna B values were recorded at gain region of 4 to 0.5 dB.

[c] Omni antenna B values at 2113.3 MHz were recorded at gain region of 4 to 0.5 dB.

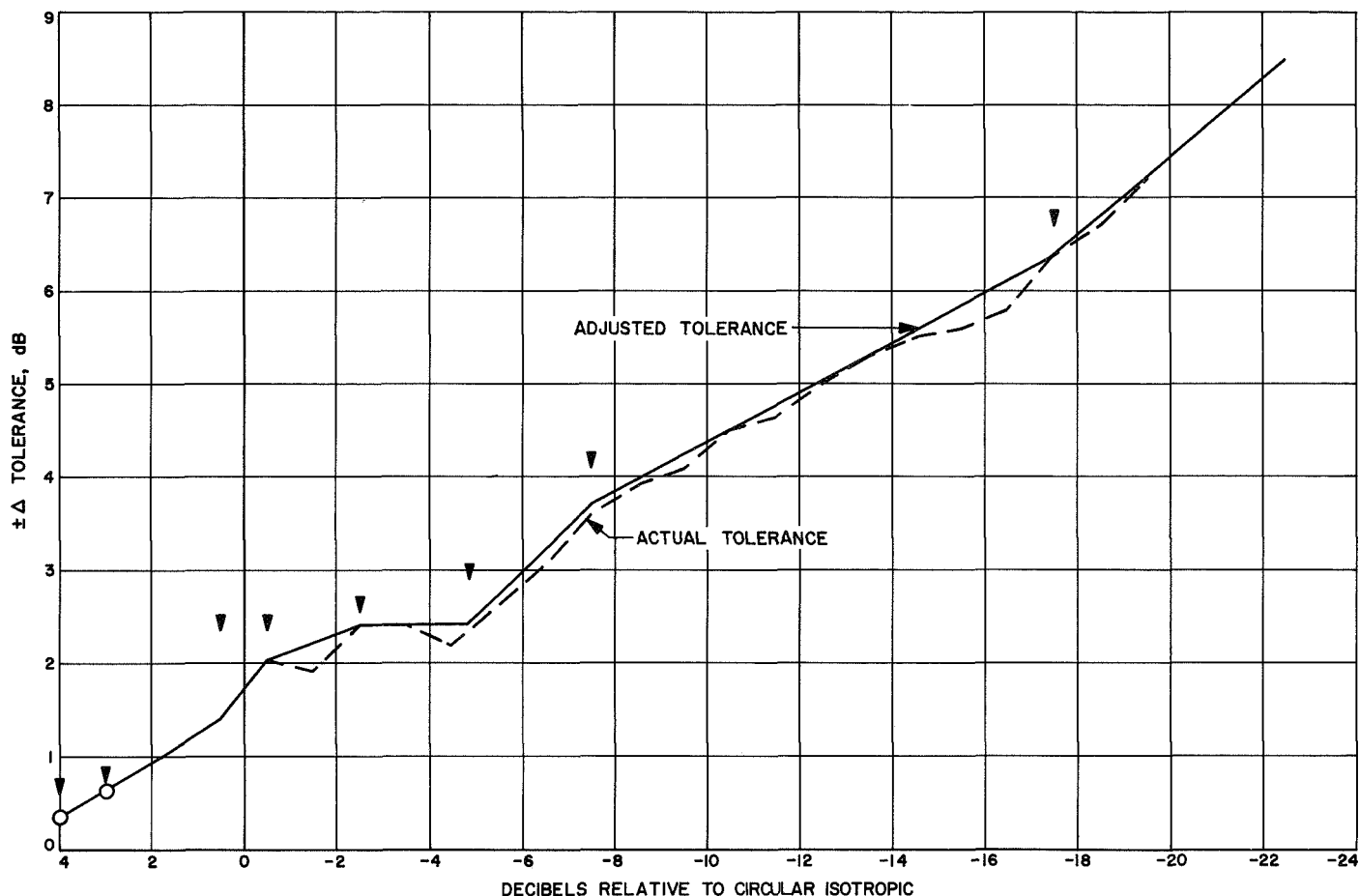[d] Totals include constant values and sectionally continuous gain values.

Fig. 16. Range tolerance as a function of absolute gain level

supplementary data in the form of *mirror image* patterns (also known as "comparison" or "roll" patterns) were recorded with the omni antennas on the spacecraft.

a. Mirror image patterns. These patterns were recorded by taking two pattern cuts with the spacecraft oriented in two different positions relative to the range. Specifically, the cuts taken were:

Cut 1 — (θ, ϕ) cw azimuth

Cut 2 — $(\theta, \phi + 180 \text{ deg})$ ccw azimuth

where $(\theta, \phi$ are not spacecraft coordinates in these measurements):

ϕ (constant angle) = 0, 45, 90, and 135 deg

ϕ = 0 (represents omni antenna axis in horizontal plane)

θ = variable angle; 0 deg $\le \theta \le$ 360 deg

For image patterns on a reflectionless range, the amplitude function for each cut must be identical. Therefore, an overlay comparison of these pattern cuts on an unknown range is a measure of the range quality. Comparisons made of the recorded data at 2295.0 and 2113.3 MHz showed that the differences between the pattern cuts described were within the envelope derived from the omni antenna prototype field probing. Since the omni antenna, during final flight type measurements, is restricted in position to the upper hemisphere about the spacecraft, the comparison patterns for the case where $(\phi = 0)$ and $(\phi = 180)$ were the only true comparison patterns. All other comparison patterns were taken as a matter of interest. As comparison patterns, they are not to be construed as valid for assessing errors, because the comparison is being made in an unrealistic flight recording condition, i.e., the antenna is *looking* towards the ground. Although the comparison patterns for ϕ other than 0 and 180 deg showed larger differences, they were not, in general, excessive. Figure 17
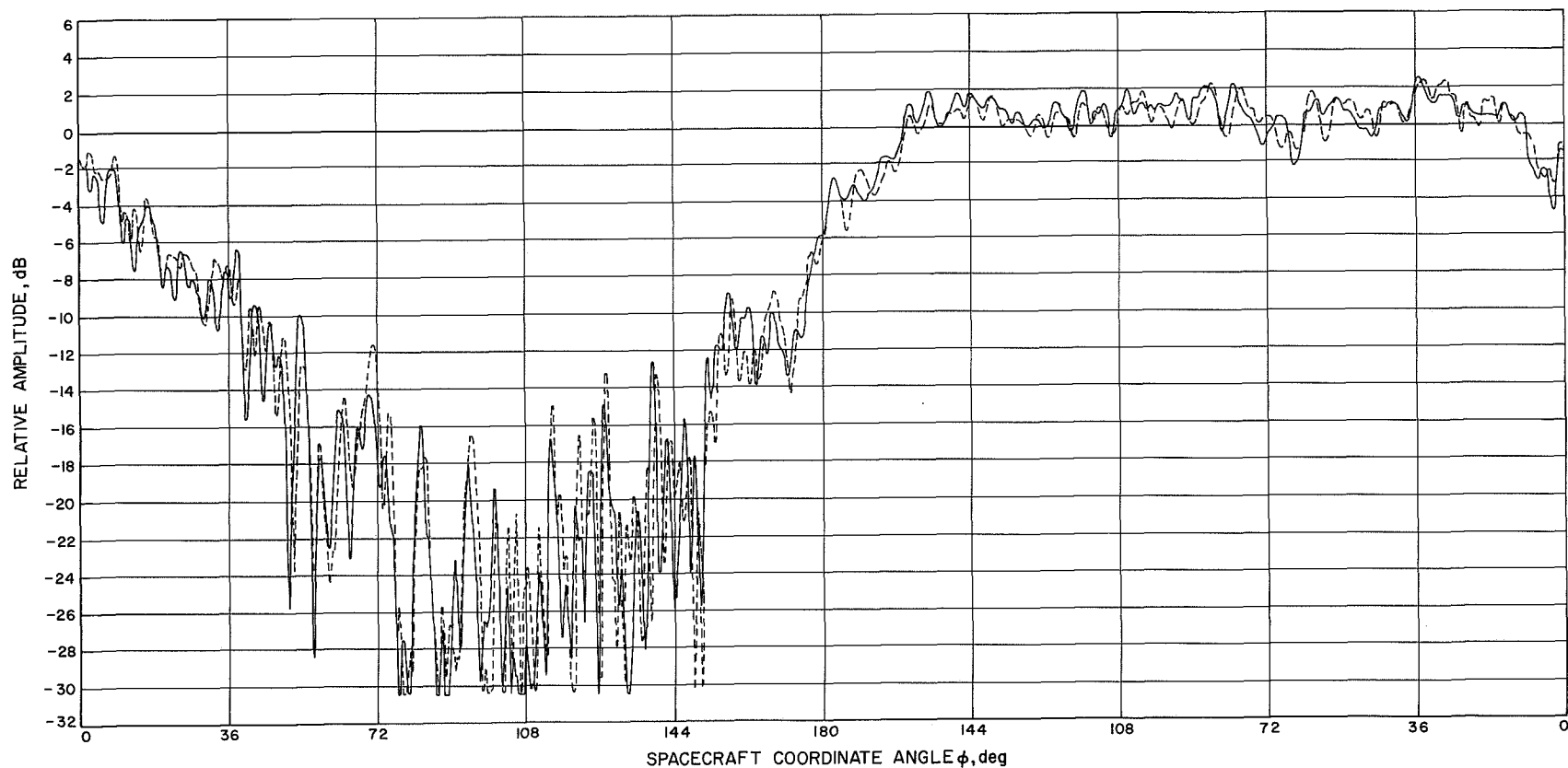
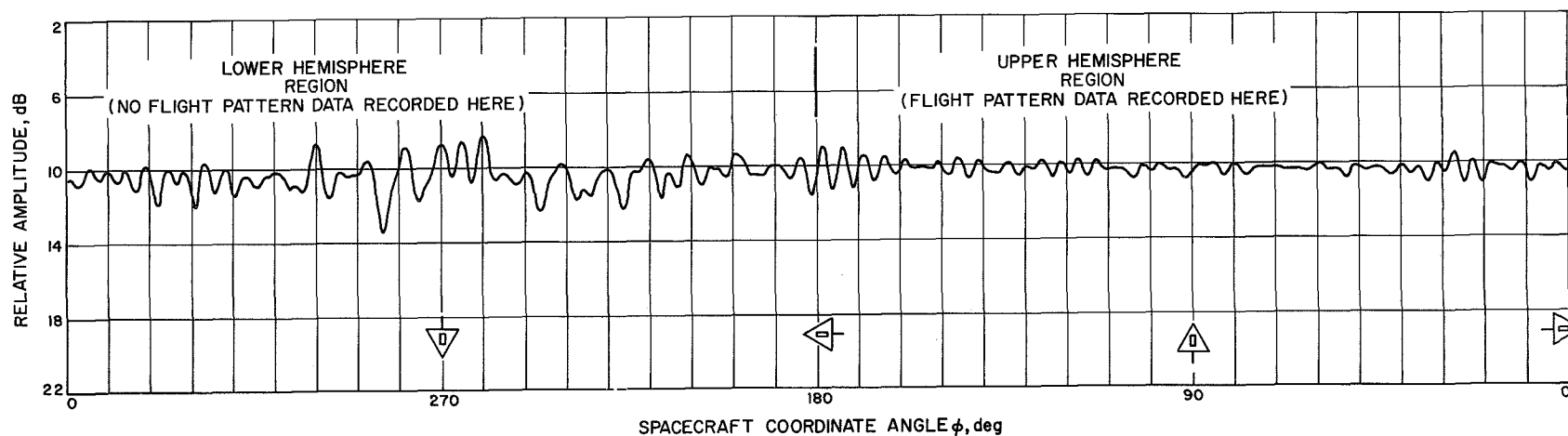Fig. 17. Comparison pattern of $\phi = 0$ deg (solid line) and $\phi = 180$ deg (dotted line)

Fig. 18. Typical spacecraft roll pattern of omni antenna A at 2295.0 MHz

shows the comparison plot for the cases of $\phi = 0$ deg and $\phi = 180$ deg.

b. Roll patterns. These patterns were recorded for the angular coordinates (0 deg, ϕ); Fig. 18 shows a typical roll pattern. Roll patterns were made with the azimuth position θ of the spacecraft held constant at 0 deg ($-z$-axis boresighted to the illuminator) while the spacecraft was rolled about its z-axis. On a *clean range*, such a pattern would display a constant amplitude as a function of ϕ (except for a polarization mismatch loss which in this case is negligible), since these coordinates represent one point on the sphere. Variations in such a pattern, therefore, are a measure of range quality.

The data recorded at 2295.0 and 2113.3 MHz showed average variations on the order of ±1.0 dB. A maximum variation of ±2.1 dB was recorded for omni antenna B at 2113.3 MHz. This value of ±2.1 dB compares favorably with the value of ±2.3 dB found by the field probing method. In Fig. 16, the range errors are seen to be ±2.3 dB at the -4.0-dB gain level. In summary, the magnitudes of the roll pattern uncertainties were within the envelope derived from the prototype omni antenna field probing.

2. Support tower absorber. To complete the range evaluation, a test was performed at 2295.0 MHz to determine the effectiveness of absorbing material in reducing currents on the support tower. These currents are excited by the illuminating field and produce secondary fields which cause errors in the pattern measurements.

A prototype omni antenna pattern was taken about the support tower while it was wrapped with a ⅛-in. thick, 10-dB insertion loss RF absorber. Comparison of this pattern with the one taken without the absorber showed negligible differences. The absorber, therefore, was not used during the measurement program.

B. Instrumentation and Calibration Tolerances

The remainder of the tolerances attributable to measurement are related to the capabilities of the instrumentation used and to the accuracy to which calibration is performed.

1. Recording system linearity. This linearity tolerance is a measure of the departure of the receiving system from a linear response as a function of gain level, and determines the recording system dynamic range. Derivation of this tolerance was accomplished by inserting,

into the input of the receiving system RF section, a continuously variable attenuator and fixed pad combination resulting in a calibrated 40-dB dynamic range. Each dB of attenuation inserted into the RF portion of the circuit results in a corresponding response at the audio end of the circuit. This response was measured in dB with an analog pen recorder. From this data, the curve of Fig. 19 was generated. An averaging process was applied to this data so that uncertainties due to pen recorder resolution would be eliminated to a first order of approximation. Measurement uncertainty due to RF attenuator calibration was considered as ±0.03 dB (as in the following antenna mismatch loss) with an additional ±0.1 dB for cascading low VSWR pads with the variable attenuator.

The receiving system linearity is seen to be a linearly increasing function of gain level. Based on a maximum linearity value of 0.38 dB (includes all uncertainties), the dynamic range at 2295.0 MHz is approximately 35.5 dB.

2. Recording system stability. This stability is a measure of the change in illuminating power level between pattern records taken at different times. Plans to monitor the total illuminating and receiving system stability prior to final flight-type measurements were partially carried out. This partial completion was due to unscheduled efforts directed to the investigation of DAP recorder and receiving electronics noise problems. Illuminator stability, however, was monitored extensively through all phases of field probing and final flight-type measurements. Illuminator stability was typically ±0.1 dB over the recording periods bounded by sunrise and sunset.

During spacecraft appendage studies, which were made after obtaining the cruise mode data (discussed
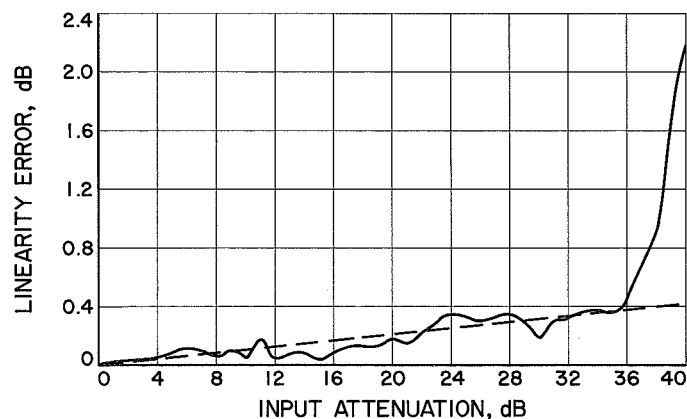

Fig. 19. Receiving system linearity calibration

later), a receiving system power drift was noticed. It was traced to a thermal control failure of the receiving system electronics. A system stability check was then run on a 24-h period, and verified the drift. On a typical recording period of approximately 2.5 to 3.0 h, a 0.25-dB power decrease occurred. An additional tolerance of ±0.25 dB has been applied to all pattern data taken, since no assurance is available that thermal control failure occurred after the final flight-type patterns were taken.

3. Recording system ellipticity stability. The ellipticity stability was established prior to the *Surveyor* program and was found to have negligible variations. The ability to repeat measurements of ellipticity magnitudes from day to day during the *Surveyor* program verified a stable polarization condition. Therefore, errors due to ellipticity stability as well as polarization mismatch were considered negligible.

4. Gain standard antenna calibration. This tolerance reflects the accuracy to which the absolute gain of a standard reference antenna can be established.

The absolute gain of a dual-polarized standard gain antenna was measured using the three-antenna method. Gain calibration data were collected in separation distance increments of a quarter wavelength over a two-wavelength distance for each of the three separation distances between antennas. The average gain at each of the three separation distances was calculated. These average gains were averaged a final time over the three separation distances. The accuracy of the Weinschel dual-channel insertion loss measurement system was then computed. This tolerance, together with the upper and lower bounds from which the final average gain was computed, constitute the tolerance on the absolute gain determination. The tolerance for each gain standard was measured to be:

Frequency, MHz	Tolerance, dB
2113.3	±0.20
2295.0	±0.15

5. Gain comparison. This tolerance accounts for the error in establishing the standard gain reference level for the spacecraft in the nonuniform illuminated field. To determine the magnitude of the error, the standard gain antenna was raised to the spacecraft gain calibration position. This placement is considered the nominal position for establishing the gain reference.

Field variation measurements as a function of height were recorded for a vertical distance of ±5 ft about the nominal gain measurement position. These measurements showed variations less than ±0.1 dB. Hence, the uncertainty in establishing gain reference levels was established as ±0.1 dB.

6. Cable insertion loss. The uncertainty of cable and calibrated pad insertion loss due to measurement inaccuracies was established by considering the absolute accuracy of the Weinschel dual-channel insertion loss circuit and the ability to repeat the insertion loss measurements. The total error established was as follows:

Source	Error, dB
Absolute accuracy	±0.02
Repeatability	±0.01
Total error	±0.03

7. Antenna mismatch loss. This tolerance accounts for the uncertainty in the mismatch loss corrections due to the inaccuracies of making VSWR measurements. For the magnitude of the VSWR measured, this measurement uncertainty was determined to be negligible.

8. Polarization loss-absolute gain calibration. This calibration accounts for the uncertainty in establishing the standard gain reference due to the unknown antenna polarization ellipse orientations and the finite ellipticities between illuminator and dual-polarized standard gain antennas. The maximum measured value of the illuminator axial ratio was 0.25 ±0.08 dB. The maximum standard gain antenna ellipticity was 0.52 ±0.12 dB. Therefore, considering the tolerance on these ellipticity values, the maximum possible mismatch loss is less than 0.005 dB, and is considered negligible.

9. Rotary joint wow. The rotary joint wow is defined as variations in the RF signal caused by rotational asymmetries of the rotary joint. These variations were measured by rotating the spacecraft about the roll axis and detecting the rotary joint RF output with a power meter. Measured variations were indistinguishable from peak-to-peak noise variations of 0.06 dB. The rotary joint wow was conservatively estimated as ±0.03 dB.

10. Azimuth turntable slip rings. This tolerance accounts for variations in the amplitude of a 1-kHz audio signal caused by the rotational asymmetries of the azimuth turntable slip rings. Measurements of these variations at varying levels of a 1-kHz audio signal were found to be negligible.

11. Spacecraft pattern stability. It is desirable to know the stability of the spacecraft configuration as the spacecraft rolls about the z-axis during the pattern measurements. Any configurational changes can directly affect the pattern detail.

In a qualitative measurement of this parameter, six spacecraft patterns, separated by angular intervals of $\Delta\phi = 45$ deg, were recorded. A reference pattern was taken for each recorded clock angle ϕ, after which the spacecraft was rolled 180 deg and agitated by rapidly changing roll directions. The spacecraft was then returned to the same angle ϕ and a second pattern was recorded in a different color ink and was compared to the reference pattern. The amplitude differences between these patterns were averaged for each angle at gain levels greater than -7.5 dB, and at gain levels less than -7.5 dB but greater than -17.5 dB. The averages of all cuts were again averaged for a single qualitative tolerance factor. The values derived are listed in the tolerance summary of Table 2.

12. Spacecraft pattern repeatability. The ability to record a spacecraft pattern and repeat this pattern at a later date was considered as a measure of the repeatability of the measurement system. The main deterrent to repeatability is the omni antenna spacecraft coordinate locations and the errors in maintaining the established angular coordinate calibrations over a period of time.

The time interval between the patterns chosen for this comparison was one month. During this time interval, the spacecraft support tower was lowered to its horizontal position, was serviced (steel surface preventive maintenance) and, then, was raised to the pattern measurement position. The repeatability tolerance was derived by overlaying the patterns recorded one-month apart and by averaging the amplitude differences. Two averages were derived, one for gain levels greater than -7.5 dB and the other for gain levels less than -7.5 dB but greater than -17.5 dB. The values recorded (Table 2) revealed that repeatability was good.

13. Wind modulation. Excessive wind conditions, producing perturbations on the antenna gain function due to mechanical vibration of spacecraft and illuminator, are considered as a tolerance contributor. No attempt was made to study in detail the effects of wind modulation on the antenna patterns. However, it was established that, for wind velocities less than 5 mph, the effect was less than ± 0.1 dB. This wind effect was determined by visually observing the analog recorder response at arbitrary points (θ, ϕ) on the sphere during wind conditions above and below 5 mph. All patterns were recorded for wind conditions less than 5 mph, and ± 0.1 dB was assigned to this tolerance factor.

14. Thermal distortions. The perturbations on the antenna gain function caused by thermal expansion of spacecraft structure and substructure were also considered as contributors to the tolerances. The complexity of the *Surveyor* structure precludes a detailed structural distortion analysis for antenna pattern purposes. The thermal distortion tolerance is, therefore, largely a guess. The majority of the cruise mode data was taken during the evening hours, and the tolerance was arbitrarily set at ± 0.0 dB. However, omni antenna A at 2295.0 MHz was measured during the hottest portion of the day. A tolerance of ± 0.2 dB was included for the omni antenna A data.

15. Test antenna interaction. This tolerance reflects the uncertainty in establishing a reference gain due to scattering interaction between illuminator and test antenna. This error was estimated negligible based on the antenna gains and separation distances involved.

C. Spacecraft Appendage Position Tolerances

A series of analog antenna patterns were recorded to determine the effects of spacecraft appendages on the antenna patterns as these appendages were placed in positions which represented the extremes of the mechanical tolerances. These effects on the antenna patterns are categorically excluded from measurement tolerances, since they represent the mechanical assembly tolerances of the flight spacecraft.

Since a number of uniconfigurational spacecraft could possibly fly using the same pattern data, the possibility of varying appendage locations must be included in the overall tolerances. The appendages considered for this study were the solar panel-planar array combination as a unit and the omni antennas.

1. Solar panel-planar array variations. Omni antennas A and B and the antenna solar panel-planar array were first positioned in their nominal spacecraft coordinate locations. Reference antenna patterns were then recorded for six different clock angles of the spacecraft. Each cut displayed a different pattern characteristic, thus the cuts are fairly representative of the total spacecraft pattern. The next step was to record patterns for the same six clock angles with the solar panel-planar array in coordinate locations which represented the minimum and maximum mechanical position tolerances. The solar panel-planar array could be individually positioned. However, it was decided to position the solar panel-planar array as a unit, since, from an antenna viewpoint, the maximum perturbational effects would, as a first approximation, occur for positions of the solar panel-planar array combination which presented a minimum and maximum effective scattering area to the omni antenna under test.

All patterns recorded for each clock angle cut were made into a composite pattern on one chart paper. Each of the six composite patterns displayed an upper and lower boundary, between which all patterns for that particular clock angle were included.

From these individual *boundary plots*, the maximum peak-to-peak variation in dB was recorded as a function of gain level. These variations were then averaged over the six clock angle cuts, again as a function of gain. To put the data in meaningful form, one-half of the average peak-to-peak variations were plotted as a function of gain level. Thus, one could expect to find, on an average basis, perturbations on the nominal gain levels as shown in Fig. 20.
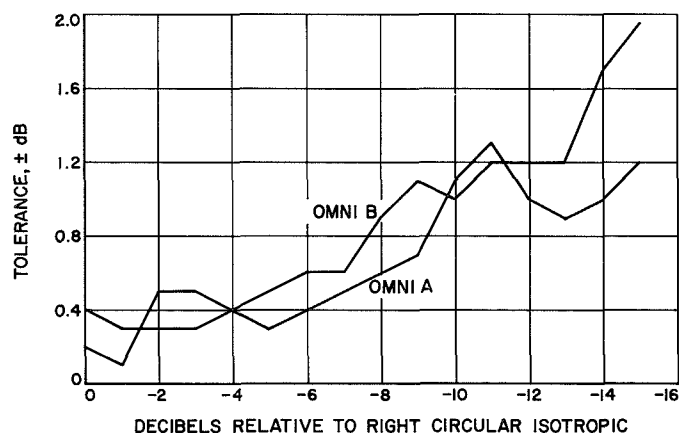

Fig 20. Solar panel-planar array variations

During the data reduction process of these perturbation studies, a 0.8 dB bias was found in the reference patterns (planar array and solar panel in nominal position). It was attributed to the recording system drift as discussed previously. The perturbation studies were typically run in the late morning hours between 9 a.m. and 12 m. The corresponding power drift variations were on the order of 0.5–1.0 dB. These variations are in contrast to the 0.25 dB during the early morning hours when flight patterns were being recorded. The curves of Fig. 15 were corrected for this drift. The corresponding curves for the omni position perturbations were derived by a lengthy statistical method and are not corrected. The curves of Figs. 21 and 22 (discussed in the next section) are slightly pessimistic, i.e., tolerances appear greater than actual, by approximately ±0.4 dB.

2. Omni antenna perturbations. A procedure similar to that used for the solar panel-planar array study was utilized to determine the effects of omni antenna movement about the nominal antenna spacecraft coordinate locations. Reference pattern data were recorded with the omni antennas in the nominal x, y, and z coordinate positions. Reference data were then recorded for spacecraft clock angles of $\phi = 269.5 + N$ (30 deg) for omni antenna A and $\phi = 59.27 + N$ (30 deg) for omni antenna B, where $N = 0, 1, 2, 3, 4,$ and 5. An attempt was then made to set the omni antennas at the extremes of their mechanical tolerance positions. This setting required guying the antenna such that its apex was on the circumference of a 1.28-in. radius circle about the nominal coordinate location. The actual omni antenna positions were limited by boom and hinge geometries; therefore, the 1.28-in. radius was not always realizable. For each of four apex locations on the tolerance circle, pattern cuts were recorded for the same clock angles at which the reference patterns were recorded.

All pattern data for each clock angle were plotted on a single chart. The data in composite form suggested that a statistical approach be used in determining the effect on the antenna pattern. A plot of one-half of the peak-to-peak variations of each individual composite pattern was made over a full 360 deg in 2-deg increments. For each of three specific gain levels, namely -5, -10, and -15 dB, tolerance levels of ±1.0, ±1.5, and ±2.0 dB were specified, respectively. The number of points sampled over 360 deg and falling within the specified tolerance at each gain level was compared with the total sample points used. For example, at the -5-dB gain level and for a tolerance of ±1.0 dB,
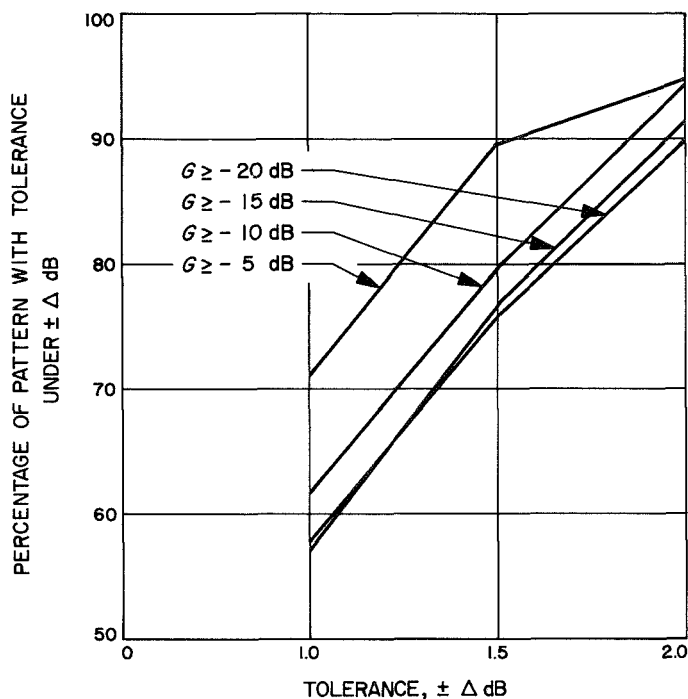
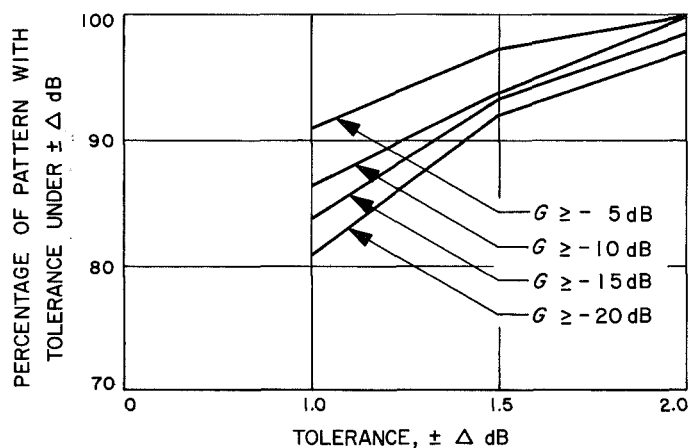**Fig. 21. Omni antenna A position tolerances**

Fig. 22. Omni antenna B position tolerances

the number of sample points falling under ±1.0 dB was compared to the total points sampled.

To make the results a function of gain level and given tolerance levels, the statistical results of the individual clock-angle composite-pattern cuts were again based on absolute gain level over all composite patterns. The final result is plotted in Figs. 21 and 22. As an example of the use of the graph, consider omni antenna A: for gain levels greater than −5 dB relative to circular isotropic, 71% of the pattern sphere has a tolerance less than or equal to ±1.0 dB, etc.

3. Omni antenna dipole orientation. Pattern data were also recorded to assess the effects of rotating the omni antenna about its conical axis. This assessment was done to determine if the pattern data recorded for the SC-1 model (dipole rotation +23 deg ccw with respect to −z-axis) could be applied to future *Surveyor* spacecraft having nominal dipole rotations of 0 deg.

A number of representative pattern cuts through the spacecraft were taken with omni antenna A rotated 23 deg ccw with respect to the −z-axis. Similar patterns were recorded for the dipole rotation at 0 deg, as per *Surveyor* specifications. Comparison of these patterns at the two angles of rotation revealed angular regions where the gain changed as much as 5–10 dB. The corresponding pattern shapes were comparable in a gross sense. Similar tests were made on omni antenna B. The omni antenna rotation angles were 4 and 0 deg, respectively. The perturbations were on the order of 1–2 dB.

D. Spacecraft Appendage Position and Manufacturing Tolerances

1. Spacecraft model and spacecraft-to-spacecraft differences. Pattern tolerances are required which reflect the spacecraft appendage and manufacturing tolerances. These tolerances can cause differences in the reflective configuration presented to the omni antennas, thus admitting the possibility of perturbing the spacecraft antenna pattern.

Without a series of flight-representative spacecraft from which to measure these differences, only an estimate can be made as to the magnitude of these perturbations. An "educated" estimate from a qualitative point of view would suggest that this tolerance factor would be a function of gain level, i.e., on a dB/dB basis, as opposed to a blanket constant. The magnitude of this tolerance was estimated to be ±(0.2 + 0.04 dB/dB).

2. Omni antenna pattern shape and absolute gain differences. Pattern shape and absolute gain differences between any two omni antennas arise from manufacturing tolerances of the antennas. To determine the magnitude of the pattern shape differences, a *free space* pattern was derived from a series of pattern measurements on the Blaine range. The particular series of patterns recorded were taken to average out the errors due to range and support structure. This recording was done for the two flight-type omni antennas available. The resultant average patterns of both antennas were then

compared, and the finite differences between them were plotted as a function of gain level. These differences were conservatively defined on a dB/dB basis by the dotted line of Fig. 23 which included all deviations. Because of the extreme low gain of the *Surveyor* antenna and the difficulty in establishing accurate *free space* patterns, the tolerance is considered as a measured estimate. Manufacturing and assembly tolerances of omni antennas were also considered to affect the on-axis gain from antenna to antenna. An estimate of the magnitude of these differences was included as ±0.2 dB in the tolerances.
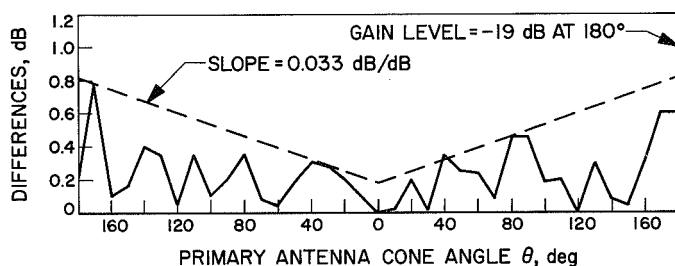

Fig. 23. Omni pattern shape differences

E. Use of Tolerance Data

The measurements made show that the mechanical positional tolerances of both the antenna solar panel and the omni antenna can be expected to perturb the gain levels of the omni antennas by the amounts shown in Figs. 20–22. In the calculation of performance margins, the tolerance data reflecting manufacturing and assembly tolerances must, according to present tolerancing philosophy, be added directly to the tolerances which reflect the uncertainty from range multipath and instrumentation errors in Table 2.

The total error, therefore, is expressed as

$$\pm\Delta\ dB = [A_m + B_{mn}(G_m - G_i)]$$

$$+ [C_m + D_{mn}(G_m - G_i)]$$

Where the use of the equation is as previously explained, A_m and B_{mn} refer to measurement type constants, and C_m and D_{mn} refer to manufacturing and assembly type constants. To determine C_m and D_{mn}, a table similar to Table 2 must be constructed for all manufacturing and assembly type tolerances.

VIII. Problems

During a data reduction process conducted by the JPL Communication Analyses Group, an oscillation appeared in a pattern plotted for the coordinates $(\theta, \phi) = (0 \deg, \phi)$ for omni antenna B at 2295.0 MHz. Although oscillations for this particular pattern were expected from range multipath errors (on a clean range, the pattern would be virtually a constant as a function of ϕ, since it represents a single point on the sphere), the oscillations for the particular pattern had a maximum peak-to-peak variation of 2.2 dB. This larger-than-expected oscillation was investigated and is believed to have been caused by a change of range recording conditions during foggy weather. (Fog conditions were prevailing during the week prior to launch when flight patterns were being recorded.)

An attempt to determine the difference in amplitude variations under wet and dry recording conditions was not realized since foggy days were not encountered during the evaluation period. However, roll patterns for both omni antennas A and B at 2295.0 MHz under dry conditions were compared with the flight pattern data. This comparison showed omni antenna B under foggy conditions to exhibit an average peak-to-peak oscillation on the order of 1.0 dB greater than under dry conditions. The comparison of the omni antenna A roll patterns revealed peak-to-peak changes of 0.1–0.5 dB, averaging out to be negligible. This comparison difference was expected since omni antenna A spacecraft patterns were taken in the dry daylight hours.

Based on the results of these comparisons and the fact that the period of the oscillations were virtually the same for dry and wet conditions (suggesting the same sources of error), a *fog* factor was included in the range reflection and diffraction tolerances for those patterns taken under foggy conditions, i.e., omni antennas A and B at 2113.0 MHz; omni antenna B at −2295.0 MHz. This factor amounts to a constant ±0.48 dB and was incorporated in the tolerance table under range reflections and diffraction.

IX. Recommendations

The net result of the omni antenna remeasurement task has been to decrease the previous measurement uncertainties from ±14.0 to ±7.5 dB at the −10-dB level.

It is estimated that this new figure represents a 3- or 4-σ uncertainty.

Although this new figure represents an improvement at the -10-dB level of a ratio of 4.5, it also implies that at the -10-dB gain level, the actual gain could be as low as -17.5 dB or as high as -2.5 dB relative to circular isotropic. The probability of realizing such gain values at the assumed -10-dB level is, in the author's opinion, negligible.

To obtain a more *realistic* picture of uncertainties for future spacecraft antenna patterns, it is recommended that a study be made on the application of statistical theory for the handling of the component uncertainties of typical antenna pattern measurements.

Abstract

With the aid of an accurate spacecraft model and the JPL calibrated antenna range, the *Surveyor* low-gain antenna pattern characteristics were remeasured with increased accuracy. Uncertainties were reduced on the order of 5.5 and 6.5 dB at the 0- and −10-dB levels, respectively.

The full-scale patterns of spherical coverage were recorded for *Surveyor* SC-1 configuration at 2295.0- and 2113.0-MHz frequencies. These patterns are on magnetic tape suitable for use in the telecommunication prediction program and are in microfilm analog form. Full-sphere patterns were also recorded at 2295.0 MHz for omni antenna A radiating in a stowed position with omni antenna B extended. Three analog *roll* patterns representing constant $\theta = 15$, 35, and 60 deg were recorded for this stowed configuration at the 2113.0-MHz frequency.

Perturbation studies were conducted at 2295.0 MHz to demonstrate the solar panel-planar array and omni mechanical position tolerances on the spacecraft patterns. For the SC-2 model, one set of full-scale patterns of spherical coverage was obtained for the omni antenna A at 2295.0 MHz in the cruise mode. No antenna pattern data were recorded for the planar array antenna.